2022

Electromechanical Mechanisms of Electromigration - Novel Approaches

Raghavendra Rao Morusupalli

University of Alabama at Birmingham

Recommended Citation

Morusupalli, Raghavendra Rao, "Electromechanical Mechanisms of Electromigration - Novel Approaches" (2022). *All ETDs from UAB*. 353.
https://digitalcommons.library.uab.edu/etd-collection/353

ELECTROMECHANICAL MECHANISMS OF ELECTROMIGRATION - NOVEL APPROACHES

by

RAGHAVENDRA RAO MORUSUPALLI

DAVID L. LITTLEFIELD, COMMITTEE CHAIR
ARIEF SURIADI BUDIMAN
S ABDOLLAH MIRBOZORGI
WILLIAM D. NIX
DEAN LEO SICKING

A Dissertation

Submitted to the graduate faculty of the University of Alabama at Birmingham, in partial fulfillment of the requirements for the degree of Doctor of Philosophy

BIRMINGHAM, AL

2022

ELECTROMECHANICAL MECHANISMS OF ELECTROMIGRATION - NOVEL APPROACHES

RAGHAVENDRA RAO MORUSUPALLI

INTERDISCIPLINARY ENGINEERING

ABSTRACT

Reliability of today's interconnect lines in microelectronic devices is critical to product lifetime. The metal interconnects are carriers of large current densities and mechanical stresses, which can cause void formation or metal extrusion into the passivation leading to failure. The modeling and simulation of stress evolution caused by electromigration in interconnect lines and vias can provide a means for predicting the time to failure of the device. Reliability and performance are equally important in the microelectronics industry of today. Product lifetimes are expected to be as high as 10 to 15 years of service. A typical microprocessor has millions of interconnect lines and the probability of line failure under operating conditions can be quite high. The interconnects in a modern microprocessor unit must be carefully engineered and tested to ensure that they are highly reliable.

Electromigration has been modeled as momentum transfer between conducting electrons and lattice atoms in a current carrying metal line. Early microelectronic devices were manufactured with large line cross-sectional areas and therefore electromigration was not an issue due to the low current densities. As devices and interconnects scaled down in feature size, the current densities became extremely large and electromigration became a key reliability concern. The current densities in modern microelectronic devices can be as high as 10 mA per square micron.

We investigate and present less researched electromechanical mechanisms that produce migration of lattice ions towards the anode of a current carrying conductor without the a priori assumption of only an electron wind force and stress gradient as driving the migration.

The work presented in this dissertation focuses on new models, their significance, new tools and newly suggested experiments to validate the derived models. We attempt to look at contemporary models of atomic flux during electromigration by incorporating forces on migrating ions that always existed but were left out in the models.

Keywords: electromigration, metals, interconnects, stress evolution, modeling, magnetic field, lorentz force, voids, morphology, experiments, simulation

ACKNOWLEDGEMENTS

There are many people to whom I owe a debt of gratitude for their kind help. However, above all, I would like to thank Professor David L. Littlefield and Professor William D. Nix. This dissertation would not have been possible without their mentoring and guidance.

I want to thank my entire committee (including Professor Dean Leo Sicking, Professor S Abdollah Mirbozorgi and Professor Arief Suriadi Budiman) for their kind help and guidance during the dissertation proposal defense and for the final approval. They provided valuable feedback and helped set appropriate limits to the scope of this dissertation.

I want to thank the entire staff at the UAB Graduate School for their excellent support and guidance throughout my time at UAB.

Finally, I want to thank the almighty God for making it possible for me to complete this program, against all odds. He brings peace to me and to our world.

TABLE OF CONTENTS

LIST OF TABLES

LIST OF FIGURES

LIST OF EQUATIONS

LIST OF SYMBOLS

$2a$	line width
Δp	Momentum transfer from electrons to the metal atoms
δx	finite difference element in length
δ	Diffusion channel width
δ_s	Thickness of the surface layer of a void
μ_0	Permeability of free space
Ω	Atomic volume
ρ	Resistivity
σ	Stress
$\triangle t$	finite difference element in time
B	Magnetic Field
B_z	Magnetic field in the Z direction
D	Diffusivity or Diffusion coefficient in m^2
D_i^o	pre-exponential constant for Diffusion along surfaces i
D_0	Maximal diffusion coefficient (at infinite temperature) in m^2/s

e	electronic charge
E_a	Activation energy for electromigration
E_t	Electric field tangent to the void surface
F_p^B	Lorentz force acting perpendicular to a void surface
F_t^e	Tangential component of the electron wind force
F_e	electron wind force
F_{EAM}	Force calculated by Embedded Atom Method (EAM)
F_{EM}	Force due to electron atom interaction
F_x	Force in the X direction
${F_x}^e$	Electron wind force in the X direction
F_y	Force in the Y direction
${F_y}^B$	Lorentz force in the Y direction
F_z	Force in the Z direction
h	line height
I	Current
J	total number of space elements
j	Current density
j	range over space increments
k	Boltzmann constant
L	line length

M	Plane strain elastic Modulus
$MTTF$	Mean Time to Failure
N	total number of time elements
n	range over time increments
N_a	Density of thermally activated lattice ions
n_e	Density of conducting electrons
q	charge
Q_i	Activation energy for Diffusion of Cu
r	Radial distance
T	Temperature in Kelvin
V	Accumulated volume
v	velocity
Z^*	charge number

SUMMARY

The present work claims the following original contributions:

- A tool was developed using MathCAD for simulation of electromigration induced stress in interconnect structures using a model of electromigration induced stress.
- Study of the effect of line geometry and overhangs on line stress evolution.
- Comparison of line stress predictions with measured electromigration failure times, useful to predict actual electromigration failures times through stress simulations.*
- Investigation of less researched magnetic and electromechanical mechanisms that would produce migration of ions towards the anode without the a priori assumption of an electron wind force and stress gradients only.*
- A novel model for atomic flux during electromigration is developed that includes intrinsically generated Lorentz forces acting on migrating lattice ions.*
- A qualitative analysis that proposes new and alternate possibilities for void morphological evolution during electromigration due to the impact of Lorentz forces on migrating ions.
- Study of the effect of current crowding on line stress evolution using MATLAB simulation tool.
- Suggestions for novel experiments that can prove the ideas theorized in the present work.*

* Work presented and published (MRS and IEEE).

These items are further elaborated as follows but detailed elsewhere in various chapters of this dissertation:

Contemporary understanding and modeling of the phenomenon of Electromigration is that of current induced transport of lattice atoms[1][2]. Accelerating electrons in a conducting line under the influence of a driving electric potential undergo collision and momentum exchange with the lattice atoms. In the presence of high current densities, an electron “wind force” is developed and momentum is transferred to atoms in the conducting material resulting in an atomic flux. This net flux causes conducting material to be depleted “up wind” and accumulated “down wind”. This depletion of material eventually leads to voids at the cathode end that cause interconnect failures. Material can also accumulate and extrude to make electrical contact with neighboring interconnect lines causing circuit malfunction.

To begin with, a tool was developed using MathCAD[3] for simulation of electromigration induced stress in VLSI interconnect structures using a model of electromigration induced stress. This model solves the equations governing atomic diffusion and stress evolution in one dimension. A numerical solution scheme has been implemented to calculate the atomic flux and the evolution of mechanical stress in interconnects. The effects of line geometries and overhangs, material properties and electromigration stress conditions have been included in the simulation. The tool has been used to simulate electromigration-induced stress in pure Cu interconnects, but it can be applied for any pure interconnect material. The tool was also used for comparing experimental data with simulated data for stress evolution in a line. Existing electromigration Time to Fail (TTF) data from studies conducted and published by Vairagar et al[4] was used to compare existing experimental electromigration data with our simulated stress data for similar test structures.

We have also investigated less researched magnetic and electromechanical mechanisms that would produce migration of ions to the anode without the a priori assumption of an electron wind force and a stress gradient only as driving the migration. This approach for electromigration flux modeling is novel and has not been researched extensively. The magnetic field is generated by flow of electrons elsewhere in the same conductor. It is not an externally applied magnetic field, but rather intrinsic to the conductor due to the flow of electrons within it. Lorentz forces acting on migrating lattice ions due to the magnetic fields are combined with electron wind force and the stress gradient to derive a new model for atomic flux. An estimation of the Lorentz forces on migrating ions for typical conditions is calculated and conditions under which the new model might be significant for electromigration damage and lifetime are presented. Conditions that make the Lorentz force significant will also result in void morphology evolution that is not necessarily in the direction of the electromigration driving force. A qualitative analysis is presented.

Further to the developed new model, we attempt to investigate how current crowding may affect electromigration adversely. Additionally, the effect of variation of the generated magnetic fields in an interconnect and resulting variations in Lorentz forces on lattice ions and their overall impact on electromigration is qualitatively analyzed. Further work is necessary to understand newly proposed phenomena such as ”lattice squeezing” due to magnetic fields on flowing electrons and a newly proposed concept of ”Dielectric drag”. These will be looked at as future work and ongoing research.

This work also includes modeling electromechanical mechanisms with the aid of simulations and modeling tools such as MATLAB[5] for stress evolution as a function of geometry and current density variations along the length of a conductor. We begin by reviewing the known effects of line geometry induced electromechanical mechanisms and current crowding on electromigration. In multilevel interconnects, current crowding occurs whenever the current changes direction, such as when passing through a via. Tu et al[6] have proposed that in current crowding, the current-density gradient can exert a driving force strong enough to cause excess vacancies (point defects) to migrate from high to low current-density regions. Electrical current crowding occurs at locations where interconnect path turns or converges, e.g. vias, sharp right angle turns etc, where the current passes from one level of the structure to another. We have attempted to simulate how abrupt geometry changes and therefore abrupt current density changes can cause corresponding changes in line stress evolution. Such simulations provide insights into potential conditions that may make the impact of Lorentz force on atomic flux a matter of significance. Further work is needed in this area and will be looked at as future and ongoing research.

Although some simulation work has been completed using Molecular Dynamics[7] (MD) tools such as LAMMPS[8], no further work in MD was planned as the intent was to apply one dimensional models using simulation tools such as MATLAB that seem to be more suitable for incorporating electron flow and thermal transport for electromigration.

Finally, experimental methods and sample fabrication techniques are suggested to study the effect of Lorentz force on defects and voids during the process of electromigration. The approach and propositions are high level recommendations. The actual conduction of the experiments or the sample fabrication is out of scope of this dissertation.

CHAPTER 1

PHYSICS OF ELECTROMIGRATION

1.1 Integrated Circuits and Interconnect Challenges

Integrated circuits of today contain millions of logic elements and circuits[9]. Human ingenuity has made it possible to package millions of circuit elements onto a tiny piece of silicon chip measuring less than half a square inch. Power consumption, cost and reliability of integrated circuits are key drivers for new design, architecture and materials research for semiconductor integrated circuit technologies. For the past forty years, there have been two major goals in the industry for the reliability of interconnect in integrated circuits. Initially it was the construction of more reliable interconnects followed by a shift in the focus for just pushing the limits of performance. Substantial progress has been made towards manufacturing reliable systems. The goal is closely linked to the improvement and the understanding of the mechanisms of electromigration failure. The reliability at operating conditions is measured by extrapolating accelerated test data[10] which is used to measure the electromigration lifetimes. This extrapolation methodology results in uncertainty in the predicted reliability performance which in turn makes design rules more conservative. An improved extrapolation scheme is therefore necessary to maximize performance and in improving the processing of interconnects. A superior and accurate extrapolation method can only be designed with a correct understanding of the details of electromigration failure mechanisms.

1.2 Electromigration Basics

Electromigration is the current induced transport of lattice atoms. Accelerating electrons in a conducting line under the influence of a driving electric potential undergo collision and momentum exchange with the lattice atoms. In the presence of high current densities, an electron “wind force” is developed and momentum is transferred to atoms in the conducting material resulting in an atomic flux[11][12]. This net flux causes conducting material to be depleted “up wind” and accumulated “down wind”. This depletion of material eventually leads to voids that cause interconnect failures. Material can also accumulate and extrude to make electrical contact with neighboring interconnect lines, and may cause circuit malfunction.

The momentum transferred by the electron wind force to a lattice atom is greatest when there is a vacancy nearby, or in the region of a grain boundary. Vacancies or grain boundaries must be present for metal atoms to move from their fixed positions in the crystal lattice[13]. In grain boundaries there is a region of distortion and open space, and the diffusion of atoms can be accommodated in these regions rather easily as compared to elsewhere in the lattice.

For aluminum, the dominant mechanism of failure due to electromigration has been attributed to atomic and vacancy diffusion along the grain boundaries. Typically, triple points of grain boundaries can serve as centers of atomic flux divergence leading to nucleation and growth of voids. For copper conductor lines, the dominant mechanism has been attributed to atomic and vacancy diffusion along the conductor surfaces and interfaces. Cu has a much higher melting point (1083^0C) compared with the melting point of Al (660^0C), so that atomic diffusion should be much slower in Cu than Al at the same temperature. Theoretically, electromigration is expected to be much less in Cu interconnects but in reality the advantage is not as big as expected. This is partly due to the fact that electromigration in Cu occurs by surface diffusion which has a lower activation energy than grain boundary diffusion. More general discussion of diffusion in solids, has been presented by Shewmon[14] and also Kaur et al[15].

1.3 Black's Law of Electromigration

It has become an industry standard to study electromigration by measurement of the mean times to failure (MTTF) of interconnect lines. In 1969, Jim Black[16] studied Al interconnect lines undergoing electromigration failure and empirically derived the following equation,

$$MTTF = \frac{A}{j^n} exp(\frac{E_a}{kT}) \tag{1.1}$$

where j is the current density, n is usually 2 for Al, T is the temperature, A is a constant that needs to be empirically determined and $E_a$is the activation energy for failure and k is Boltzmann's constant. The key feature of Black's equation is the dependence of the MTTF on the square power of current density, i.e., $n = 2$. The actual value of n to be used varies and is determined by electromigration experiments at accelerated temperatures and is a function of the type of diffusion mechanism that is dominant in causing the failure of a particular conducting material.

Above room temperature, it is inevitable that a lattice has point defects (vacancies and interstitials), grain boundaries (between crystals of differing orientation) and dangling atomic bonds at the surfaces and bulk interfaces. Phonons (atomic vibrations) exist at room temperature and become increasingly important as the temperature rises. Phonons cause electron scattering and momentum transfer. It takes time and sufficient momentum exchange to cause atom and vacancy diffusion leading to the formation of voids or extrusions in metals. The presence of lattice defects and phonons (and therefore higher temperatures) can accelerate the failure caused by electromigration.

Black's law provides basic empirically derived insight into electromigration failure, however, it does not provide a complete understanding of the underlying mechanisms related to the electromigration behavior for which more detailed physically based models such as that presented by Gleixner and Nix[17] are useful for additional insights.

1.4 Electromigration and Stress

In an interconnect line with blocking boundaries, the effect of electromigration is to deplete atoms on the cathode side while causing the atoms to accumulate on the anode. As atoms and vacancies diffuse towards the opposite ends in an interconnect, voids will begin to form at the cathode when there is no source of atoms to fill a vacancy that has reached the cathode. This results in the build-up of tensile stress at the cathode and compressive stresses at the anode end[18]. When the tensile stress at the cathode exceeds the critical stress necessary for void nucleation, a void will nucleate and begin to grow (Figure 1.1). Eventually the size of the void increases and leads to a resistance increase of the interconnect line leading to failure[19].

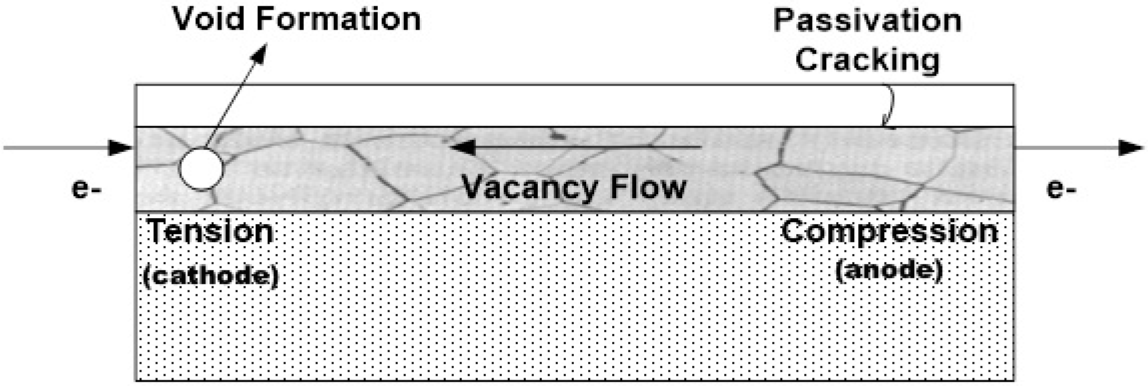

Figure 1.1: Illustration of electromigration, void formation and passivation cracking for a passivated metal line with grain-boundary textures and subjected to high current density.

To analyze the stress evolution precisely, numerical simulations are necessary. The simulation of these stresses is presented in detail in the next chapters.

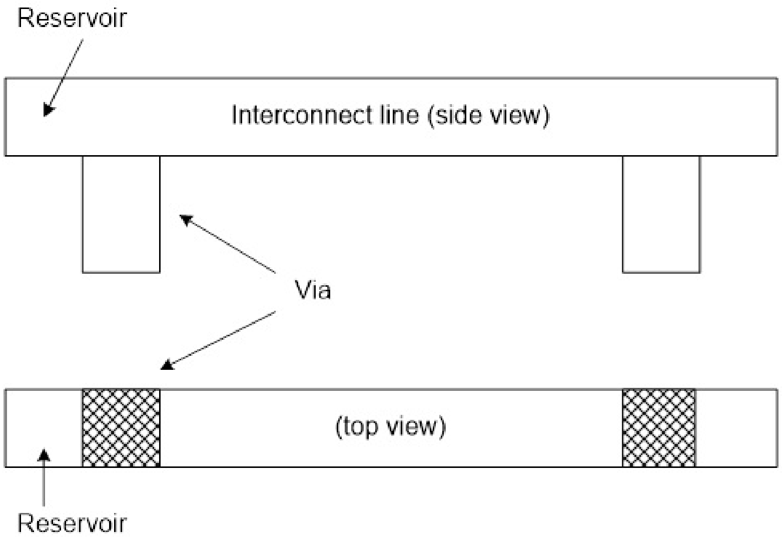

Figure 1.2: Interconnect line with vias and overhangs.

1.5 The Reservoir Effect

A reservoir is an extension (overhang) of the interconnect metal line beyond the vias (Figure 1.2). For a simple interconnect structure with two vias and a metal line with overhangs at the ends beyond the vias, the metal line does not carry any current in the overhangs. It has been shown that the lattice atoms in the reservoir, migrate in the absence of an electric field to replenish vacant sites in the non-overhang portions of the metal line and under the vias. This effect is called the reservoir effect and it has been known to improve the electromigration lifetime of line-via structures[19][20]. The motion of host atoms toward the via is in general driven by a concentration gradient and a stress gradient[20][21]. In addition, via electromigration lifetime has been shown to be a strong function of the reservoir length under fixed testing conditions[19].

CHAPTER 2

REVIEW OF ELECTROMIGRATION MODELS

2.1 Black's Model

Jim Black[11] was first to derive an equation for the mean time to failure (MTTF) of a metal line subjected to Electromigration. In the late sixties, Jim Black of Motorola was involved in understanding the line voiding problem that was later termed as electromigration. Jim's pioneering work included the first careful systematic investigations of electromigration failure kinetics. His experiments uncovered the curious behavior that electromigration failures followed kinetics that depended not on the inverse of the current density, but on the inverse square.

$$MTTF = \frac{A}{j^n} exp\left(\frac{E_a}{kT}\right) \tag{2.1}$$

where MTTF is the mean time to failure in a distribution of samples, A is a constant that needs to be empirically determined and E_a is the activation energy. The experimental values found for the activation energy suggested grain boundary diffusion as the mass transport mechanism for metals such as Al however it can be the activation energy attributed to surface diffusion for other metals such as Cu. For nucleation dominated failure, this equation has proven to be adequate even to the present day. Only small corrections, often too small to be detected experimentally, have been needed to keep Black's Law consistent with the latest theoretical developments. Jim Black started with the assumption that the mean time to failure (MTTF) depended inversely on the rate of mass transport R_m

$$MTTF \propto \frac{1}{R_m} \tag{2.2}$$

R_m is in turn proportional to the momentum transfer between conduction and thermally activated electrons,

$$R_m \propto n_e \Delta p N_a \tag{2.3}$$

where n_e is the density of conducting electrons, Δp is the momentum transfer from electrons to the metal atoms and N_a is the density of thermally activated ions. Since the electron density and momentum transfer are proportional to the amount of current density j, and the activated ions follow an Arrhenius equation,

$$n_e \propto j, \;\; \Delta p \propto j \tag{2.4}$$

$$N_a \propto exp\left(\frac{-E_a}{kT}\right) \tag{2.5}$$

the MTTF can therefore be modeled as

$$MTTF = \frac{A}{j^2} exp\left(\frac{E_a}{kT}\right) \tag{2.6}$$

where A is a constant that depends on the interconnect geometry and choice of material[11][16]. It has been established through various experimental results[22] that the current density function not always follows a fixed exponent and can therefore be modeled with a variable value of n. The modified and more general version of Black's law can therefore be expressed as,

$$MTTF = \frac{A}{j^n} exp\left(\frac{E_a}{kT}\right) \tag{2.7}$$

The actual value of n depends on the experimental conditions and needs to be determined. Various experimental and theoretical works[23][24][25] have provided values for the exponent n and its physical significance. A n value of 1 indicates a failure mechanism that is dominated by void growth[26], whereas a n value of 2 can be explained instead by a mechanism that is dominated by void nucleation[23].

CHAPTER 3

MODELING OF LINE STRESS

3.1 Description of the Model

A description of the model is given here. The line structure is idealized as shown in Fig. 1.1. As shown in the figure, the length of the line is L, the width of the line is $2a$ and the thickness of the line is h. Neither the passivation on top of the line nor the substrate below the line are shown. Atomic transport is assumed to occur along the top (and/or bottom) surfaces of the line. The thickness of the interfacial region in which transport occurs, denoted as δ is greatly exaggerated in Figure 3.1. [27].

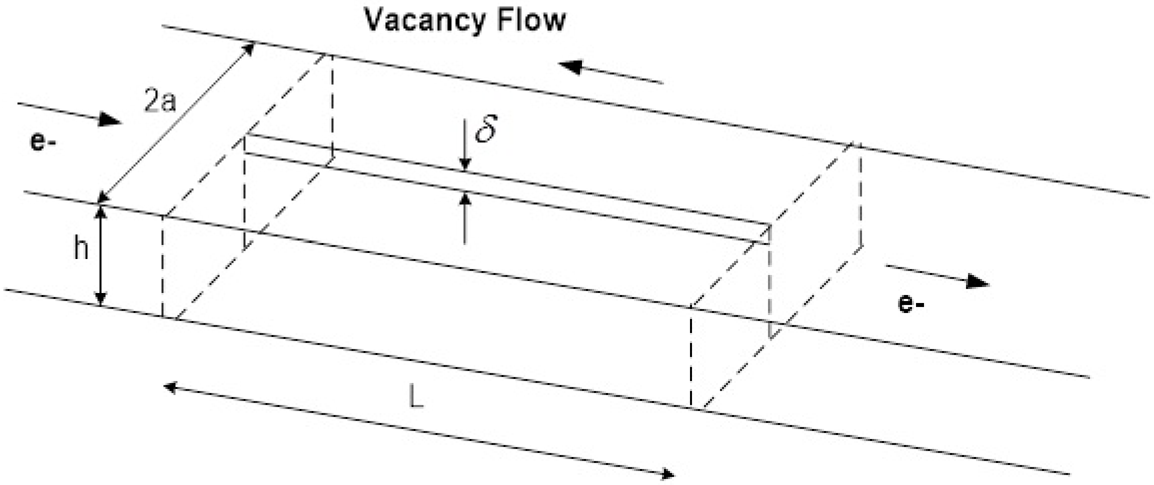

Figure 3.1: Schematic diagram of a simple interconnect line structure. Atomic transport is assumed to occur along the top (and or bottom) surface of the line. The thickness of the interfacial region in which transport occurs, denoted as δ is greatly exaggerated in the figure.

3.2 Analysis of the Model

For the present analysis, the transport along the edges of the line is ignored. The atomic flux along the top and/or bottom interfaces in the presence of both a stress gradient and electron wind may be expressed as per Huntington[28]

$$J_a^i = \frac{D_i}{kT}\left[\frac{\partial \sigma_n^i}{\partial x} + \frac{F_e}{\Omega}\right] \tag{3.1}$$

where i stands for either the top or bottom surface of the line. The atomic diffusivity is given by

$$D_i = D_i^o exp\left(-\frac{Q_i}{kT}\right) \tag{3.2}$$

where Q_i is the activation energy for diffusion along the interface and D_i^o is the pre-exponential constant. As discussed below, consider the interfacial diffusion to be bounded by the limits of grain boundary diffusion at the lower end and surface diffusion at the upper end. Also, F_e is the electron wind force in the direction of the current flow given by

$$F_e = -eZ^* \rho j \tag{3.3}$$

where eZ^* is the effective charge on the ions, ρ is the resistivity of the metal line and j is the current density[28][17].

In the present treatment the mass and/or vacancy flow into or out of the crystal lattice is ignored. An analysis that takes these factors into account has not been developed. The accumulation of mass at the interface may be computed using a mass balance. This leads to the expression for the volume of mass accumulation V at a given point along the interface

$$\frac{\partial V}{\partial x} = -2a\Omega\delta\frac{\partial J_a^i}{\partial x} \tag{3.4}$$

where Ω is the atomic volume. The accumulation of matter at any point along the interface causes the two sides of the interface (the line and the passivation, for example) to be displaced away from each other, leading to a pressure in the interface. As discussed by Gleixner and Nix[17], insertion of matter at an interface can be treated like a pressurized crack of length $2a$. According to this treatment the form of the normal displacements at the interface is

$$u_z(y) = 4\left(\frac{p}{M}\right)\sqrt{a^2 - y^2} \tag{3.5}$$

where p is the pressure in the interface and M is the plane strain elastic modulus of the surrounding material. Also, the corresponding area of the opened crack is

$$A = 4\pi a^2\left(\frac{p}{M}\right) \tag{3.6}$$

The gradient in the rate of volume accumulation V at a given point along the interface is simply the rate of change of the opened area given by

$$\frac{\partial V}{\partial x} = -2a\Omega\delta\frac{\partial J_a^i}{\partial x} = \dot{A} \tag{3.7}$$

where the area displacement rate is,

$$\dot{A} = 4\pi a^2\frac{1}{M}\frac{\partial p}{\partial t} \tag{3.8}$$

But since the normal stress in the interface is $\sigma_n^i = -p$ (tension is negative pressure) it follows that

$$\dot{A} = -4\pi a^2 \frac{1}{M} \frac{\partial \sigma_n^i}{\partial t} \tag{3.9}$$

Thus, combining equations (3.7) and (3.9) the governing equation is

$$4\pi a^2 \frac{1}{M} \frac{\partial \sigma_n^i}{\partial t} = 2a\Omega\delta \frac{\partial J_a^i}{\partial x} \tag{3.10}$$

and combining with equation (3.1),

$$\frac{2\pi a}{\Omega\delta M} \frac{\partial \sigma_n^i}{\partial t} = \frac{\partial}{\partial x} \frac{D_i}{kT} \left[\frac{\partial \sigma_n^i}{\partial x} + \frac{F_e}{\Omega} \right] \tag{3.11}$$

Equation 3.11 is the partial differential equation (PDE) for computing the stress evolution in the line. This PDE is solved numerically in the MathCAD tool that has been developed. Initially the stress in the line is assumed to be zero. Then, as current flows in the line, a stress develops according to Equation 3.11. Naturally the stresses develop first at the ends of the line where diffusion is blocked. Gradually a stress gradient develops everywhere in the line. Eventually, at long enough times, a linear, steady state, stress gradient develops.

The most uncertain parameter in the model is the diffusivity in the interface. To estimate the stresses it is assumed that the interfacial diffusivity is bounded by grain boundary and surface diffusivity. In particular, the tool allows one to assume either grain boundary diffusion or surface diffusion for the diffusivity. Naturally, the stresses develop more quickly if surface diffusion is assumed and more slowly if grain boundary diffusion is assumed. The interfacial diffusivity might be lower than grain boundary diffusivity but it is not likely any higher than surface diffusion.

CHAPTER 4

NUMERICAL IMPLEMENTATION

This chapter presents the details of the numerical implementation of the partial differential Equation 3.11. The method of finite difference equations has been used for the numerical implementation.

4.1 Derivation of Finite Difference Equations

The basic idea of the finite differences method of solving a PDE is to replace spatial and time derivatives by suitable approximations, then to numerically solve the resulting difference equations. Consider a function $f(x,t)$. Instead of solving for the conditions where x and t are continuous, let us consider solving for $f_{j,n} = f(x_j, t_n)$ where x and t represent space and time dimensions respectively.

Imagine a grid system shown in Figure 4.1, where the point labeled j, n corresponds to $(x,t) = (x_j, t_n)$. The derivatives of f can be approximated in terms of the values of f at grid points. For example, it is known that

$$\frac{\partial f}{\partial x} = \lim_{\triangle x \to 0} \frac{\triangle f}{\triangle x} \tag{4.1}$$

This derivative at the grid-point $(x,t) = (x_j, t_n)$ can be approximated in the following

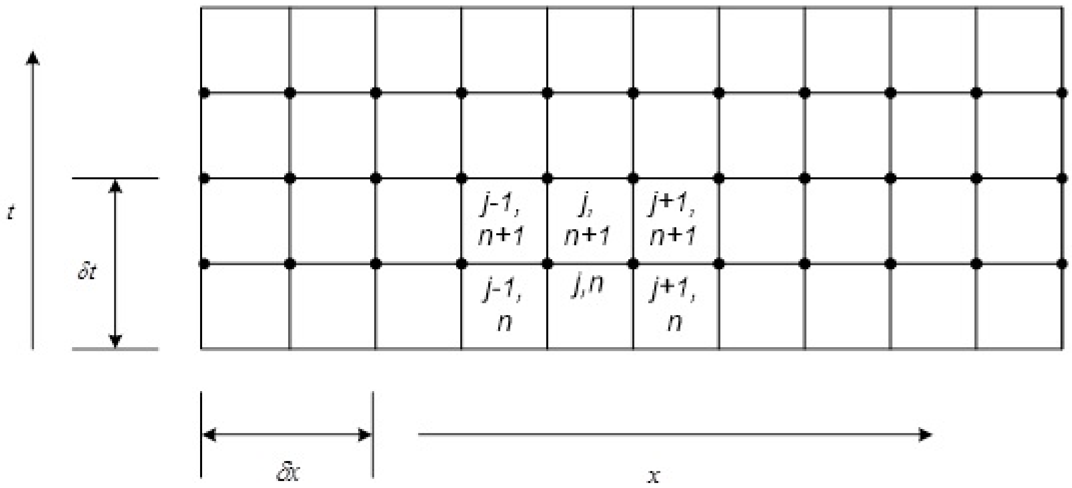

Figure 4.1: Imaginary grid system for the Finite Differences

different ways:

$$\left.\frac{\partial f}{\partial x}\right|_{x_j,t_n} = \frac{f_{j+1,n} - f_{j,n}}{x_{j+1} - x_j} = \frac{f_{j+1,n} - f_{j,n}}{\delta x} \tag{4.2}$$

which is called the forward difference. The derivative can also be approximated as a backward difference as shown below:

$$\left.\frac{\partial f}{\partial x}\right|_{x_j,t_n} = \frac{f_{j,n} - f_{j-1,n}}{x_j - x_{j-1}} = \frac{f_{j,n} - f_{j-1,n}}{\delta x} \tag{4.3}$$

In this treatment the forward difference equation for the numerical implementation has been used.

The second derivative at the grid-point $(x, t) = (x_j, t_n)$ can be approximated as:

$$\frac{\partial^2 x}{\partial x^2} = \lim_{\triangle x \to 0} \frac{\triangle\left(\frac{\partial f}{\partial x}\right)}{\triangle x}$$

This equation for the second derivative at the grid-point $(x, t) = (x_j, t_n)$ can be approximated using the finite difference expression:

$$\left.\frac{\partial^2 f}{\partial x^2}\right|_{x_j,t_n} = \frac{f_{j+1,n} - 2f_{j,n} + f_{j-1,n}}{(\triangle x)^2} \tag{4.4}$$

With the difference equations methodology developed so far for the first and second derivatives of a general function f, it is now possible to express the PDE using difference equations.

4.2 Implementation without Overhang Elements

The interconnect can be represented by a finite difference element model as shown in Figure 4.2. Consider the opposite sides of the interconnect as being mass-blocking. Several variables are introduced as defined below:

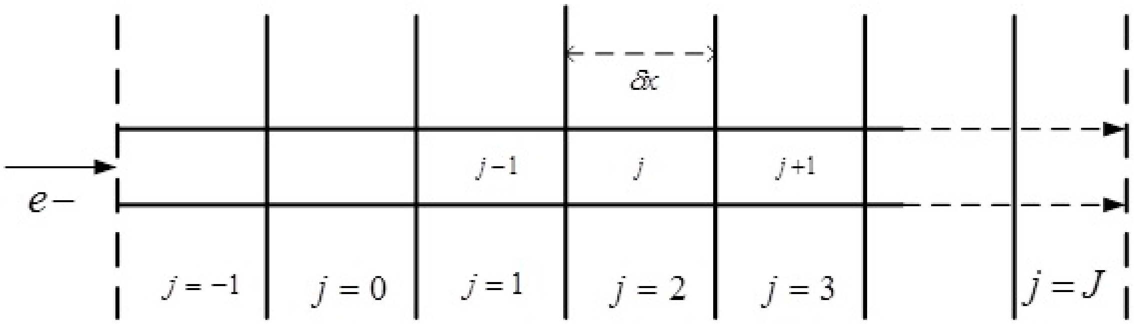

Figure 4.2: Interconnect line represented by finite difference elements

j := 0, 1, . . . , J . . . ranges over space increments - Finite elements
n := 0, 1, . . . , N . . . ranges over time increments

Consider flux from cell j to cell $j + 1$ in the finite element representation of Fig 4.1

$$J_{j\to j+1} = \frac{D}{kT}\left[\left(\frac{\sigma_{n,j+1} - \sigma_{n,j}}{\delta x}\right) + \frac{F_e}{\Omega}\right] \tag{4.5}$$

Now, for flux change from cell $j-1$ to cell j is given by:

$$J_{j-1\to j} = \frac{D}{kT}\left[\left(\frac{\sigma_{n,j}-\sigma_{n,j-1}}{\delta x}\right)+\frac{F_e}{\Omega}\right] \tag{4.6}$$

Volume Accumulation rate at cell j can be shown to be equal to:

$$\delta V_j = \delta 2a\Omega[J_{j-1\to j} - J_{j\to j+1}] \tag{4.7}$$

The area rate at the cell j is:

$$\dot{A}_j = \frac{\delta V_j}{\delta x} \tag{4.8}$$

By using the pressurized crack model referred to in chapter 2, it can be shown that:

$$\dot{A}_j = -4\pi a^2\frac{1}{M}\left(\frac{\sigma_{n+1,j}-\sigma_{n,j}}{\triangle t}\right) = \delta 2a\Omega\frac{1}{\delta x}[J_{j-1\to j} - J_{j\to j+1}] \tag{4.9}$$

and therefore, inserting Eq 4.5 and Eq 4.6 into Eq 4.9 and using simple algebra shown below for Eq 4.10 thru Eq 4.13, the stress evolution expression of Eq 4.14 can be easily derived:

$$\frac{-2\pi a}{\delta\Omega M}\left(\frac{\sigma_{n+1,j}-\sigma_{n,j}}{\triangle t}\right) = \frac{1}{\delta x}[J_{j-1\to j} - J_{j\to j+1}] \tag{4.10}$$

$$\frac{-2\pi a}{\delta\Omega M}\left(\frac{\sigma_{n+1,j}-\sigma_{n,j}}{\triangle t}\right) = \frac{1}{\delta x}\times\frac{D}{KT}\left[\frac{\sigma_{n,j}-\sigma_{n,j-1}}{\delta x}+\frac{F_e}{\Omega}-\frac{\sigma_{n,j+1}-\sigma_{n,j}}{\delta x}-\frac{F_e}{\Omega}\right] \tag{4.11}$$

$$\frac{-2\pi a}{8\Omega M}\left(\frac{\sigma_{n+1,j}-\sigma_{n,j}}{\triangle t}\right)=\frac{D}{KT}\left[\frac{\sigma_{n,j}-\sigma_{n,j-1}-\sigma_{n,j+1}+\sigma_{n,j}}{(\delta x)^2}\right] \tag{4.12}$$

$$\frac{\sigma_{n+1,j}-\sigma_{n,j}}{\triangle t}=\frac{\delta\Omega MD}{2\pi akT}\left[\frac{\sigma_{n,j+1}-2\sigma_{n,j}+\sigma_{n,j-1}}{(\delta x)^2}\right] \tag{4.13}$$

$$\sigma_{n+1,j}=\sigma_{n,j}+\beta\triangle t\left(\frac{\sigma_{n,j+1}-2\sigma_{n,j}+\sigma_{n,j-1}}{(\delta x)^2}\right) \tag{4.14}$$

where $\beta=\frac{\delta\Omega MD}{2\pi akT}$

This applies to an arbitrary point where $j \neq 0$ and $j \neq J$. This is an expression for the time evolution of the line stress state for an arbitrary point not including the ends.

Using a similar analysis, it can be shown that for the element represented by $j = 0$ the time evolution of line stress is be given by:

$$\sigma_{n+1,0}=\sigma_{n,0}+\beta\triangle t\left(\frac{\sigma_{n,1}-\sigma_{n,0}}{(\delta x)^2}+\frac{F_e/\Omega}{\delta x}\right) \tag{4.15}$$

and for the element represented by $j = J$, the time evolution of the line stress is given by:

$$\sigma_{n+1,J}=\sigma_{n,J}+\beta\triangle t\left(\frac{\sigma_{n,J}-\sigma_{n,J-1}}{(\delta x)^2}+\frac{F_e/\Omega}{\delta x}\right) \tag{4.16}$$

Equations (4.14) thru (4.16) are an explicit numerical implementation because the computation of σ at $time = n + 1$ is completely determined by our computation of σ at

$time = n$. This scheme is also called *consistent* because the finite difference approximations have a truncation error that approaches zero in the limit that $\delta t \to 0$ and $\delta x \to 0$.

Although this is a consistent method, it is still not guaranteed that iterating the stress state difference equations (4.14) thru (4.16) will give a good approximation to the true solution of the stress equation. The numerical implementation will be fully convergent when the solution of the stress equation approaches the exact solution.

The issue of *convergence* is related to the issue of *stability* of the numerical implementation. (the implementation will be *conditionally stable* if it does not magnify errors that arise in the course of the calculations). For a linear PDE, and a consistent finite difference approximation, stability is the necessary and sufficient condition for convergence. It can be shown that the numerical implementations given by equations (4.14) thru (4.16) are only convergent when the following conditional stability criterion is met[17].

$$D\frac{\delta t}{(\delta x)^2} \leq 0.5 \tag{4.17}$$

The stability criteria described above has been carefully incorporated into the numerical implementation and a balance has been worked between speed, accuracy, stability and practicability. Details of a MathCAD implementation of the PDE using difference equations is presented in the next chapter. It uses the following initial and boundary conditions for a pure copper interconnect with two mass blocking ends:

$IC : \sigma_{0,j} = 0$

i.e. at time $time = 0$, stress $\sigma_{0,j}$ = 0.

$BC : J_{-1 \to 0} = 0$ and $J_{J \to J+1} = 0$

i.e. for insulating line ends $j = 0$ and $j = J$, the flux in and flux out are zero respectively.

4.3 Implementation with Overhang Elements

This is the case of a pure copper interconnect with two mass blocking ends as part of overhang: This can be represented schematically as shown below in Figure 4.3. In the schematic of Figure 4.2. the finite elements before the elements represented by $j = 1$ and after $j = J - 1$ are overhangs and a analysis of the net flux for these elements would show that these special elements have stress relations described by the following equations:

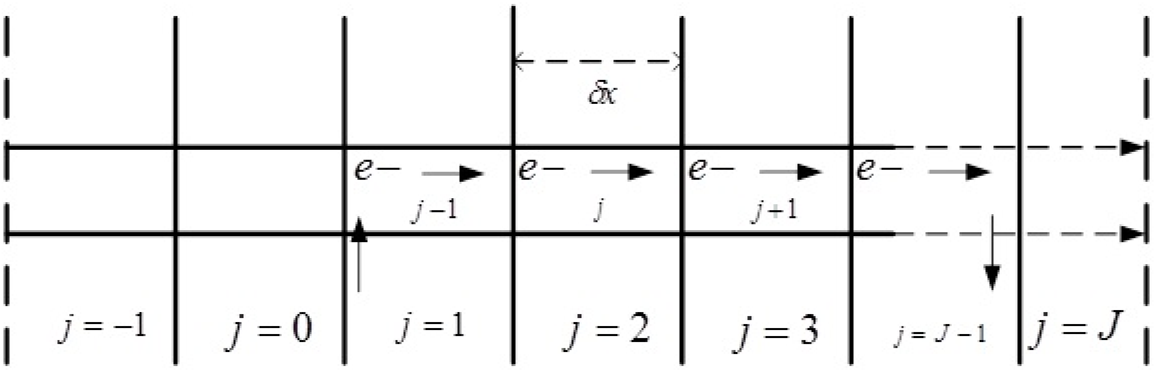

Figure 4.3: Interconnect line represented by finite difference elements with end overhang elements.

$$\sigma_{n+1,j} = \sigma_{n,j} + \beta\triangle t\left(\left(\frac{\sigma_{n,j+1} - 2\sigma_{n,j} + \sigma_{n,j-1}}{(\delta x)^2}\right) + \frac{F_e/\Omega}{\delta x}\right) for\ j = 1 \tag{4.18}$$

and

$$\sigma_{n+1,j} = \sigma_{n,j} + \beta\triangle t\left(\left(\frac{\sigma_{n,j+1} - 2\sigma_{n,j} + \sigma_{n,j-1}}{(\delta x)^2}\right) - \frac{F_e/\Omega}{\delta x}\right) for\ j = J - 1 \tag{4.19}$$

$IC : \sigma_{0,J} = 0$

i.e. at time $time = 0$, stress $\sigma_{0,J} = 0$, everywhere.

$BC : J_{-1\to 0} = 0$ and $J_{J\to J+1} = 0$

i.e. for insulating line ends $j = 0$ and $j = J$, the flux in and flux out are zero respectively. The boundary condition for the overhang case is extended to all elements which are part of the overhang. The implementation is shown in the next chapter.

The size of the overhang can be varied by choosing the appropriate position of the special finite difference element(s).

In the MathCAD implementation described in the next chapter, non-dimensional forms of the difference equations have been used.

CHAPTER 5

MATHCAD IMPLEMENTATION

5.1 Basic Assumptions

The MathCAD implementation of the PDE Equations involve some basic assumptions.

Throughout the implementation the interconnect material is assumed to be pure Copper element with the following material properties[17][29]

$Atomic\,Volume\,\Omega = 1.18 \times 10^{-29}\,Cubic\,Meters$

$Plane\,Strain\,Modulus\,M = 7 \times 10^{10}\,Pa$

$Thickness\,of\,Interface\,\delta = 1 \times 10^{-9}\,Meters$

$Resistivity\,\rho = 1.7 \times 10^{-8}\,Ohm - Meters$

$Effective\,Charge\,Number\,Z = 4$

The Line geometry was assumed to have the following dimensions:

Line length L = 70 microns

Line width 2a = 0.56 microns

Line thickness h = 0.97 microns

Two limiting cases of Cu diffusivity D_{0i} are assumed[29]

Table 5.1: Assumed values for Cu interconnect

	D_{0i}	Q_i
Cu GB Diffusion	5×10^{-6}	104 KJ per mole
Cu Surface Diffusion	15×10^{-6}	86.65 KJ per mole

5.2 Implementation Without Overhang

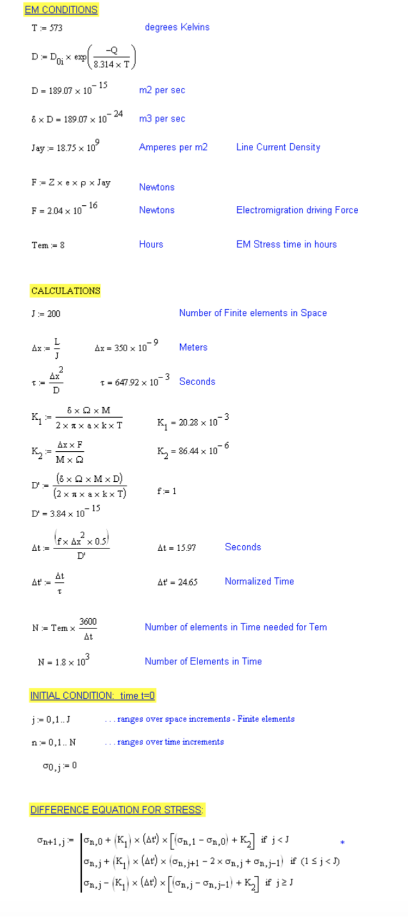

EM CONDITIONS

$T := 573$ degrees Kelvins

$D := D_{0i} \times \exp\left(\frac{-Q}{8.314 \times T}\right)$

$D = 189.07 \times 10^{-15}$ m2 per sec

$\delta \times D = 189.07 \times 10^{-24}$ m3 per sec

$Jay := 18.75 \times 10^{9}$ Amperes per m2 Line Current Density

$F := Z \times e \times \rho \times Jay$ Newtons

$F = 2.04 \times 10^{-16}$ Newtons Electromigration driving Force

$Tem := 8$ Hours EM Stress time in hours

CALCULATIONS

$J := 200$ Number of Finite elements in Space

$\Delta x := \frac{L}{J}$ $\Delta x = 350 \times 10^{-9}$ Meters

$\tau := \frac{\Delta x^2}{D}$ $\tau = 647.92 \times 10^{-3}$ Seconds

$K_1 := \frac{\delta \times \Omega \times M}{2 \times \pi \times a \times k \times T}$ $K_1 = 20.28 \times 10^{-3}$

$K_2 := \frac{\Delta x \times F}{M \times \Omega}$ $K_2 = 86.44 \times 10^{-6}$

$D' := \frac{(\delta \times \Omega \times M \times D)}{(2 \times \pi \times a \times k \times T)}$ $f := 1$

$D' = 3.84 \times 10^{-15}$

$\Delta t := \frac{(f \times \Delta x^2 \times 0.5)}{D'}$ $\Delta t = 15.97$ Seconds

$\Delta t' := \frac{\Delta t}{\tau}$ $\Delta t' = 24.65$ Normalized Time

$N := Tem \times \frac{3600}{\Delta t}$ Number of elements in Time needed for Tem

$N = 1.8 \times 10^{3}$ Number of Elements in Time

INITIAL CONDITION: time t=0

$j := 0,1..J$ ...ranges over space increments - Finite elements

$n := 0,1..N$ ...ranges over time increments

$\sigma_{0,j} := 0$

DIFFERENCE EQUATION FOR STRESS:

$$\sigma_{n+1,j} := \left| \begin{array}{l} \sigma_{n,0} + (K_1) \times (\Delta t') \times [(\sigma_{n,1} - \sigma_{n,0}) + K_2] \text{ if } j < J \\ \sigma_{n,j} + (K_1) \times (\Delta t') \times (\sigma_{n,j+1} - 2 \times \sigma_{n,j} + \sigma_{n,j-1}) \text{ if } (1 \le j < J) \\ \sigma_{n,j} - (K_1) \times (\Delta t') \times [(\sigma_{n,j} - \sigma_{n,j-1}) + K_2] \text{ if } j \ge J \end{array} \right.$$

Figure 5.1: MathCAD implementation for stress evolution equation for 300^0C at a current density of 18.75 mA per square micron.

5.3 Implementation With Overhang

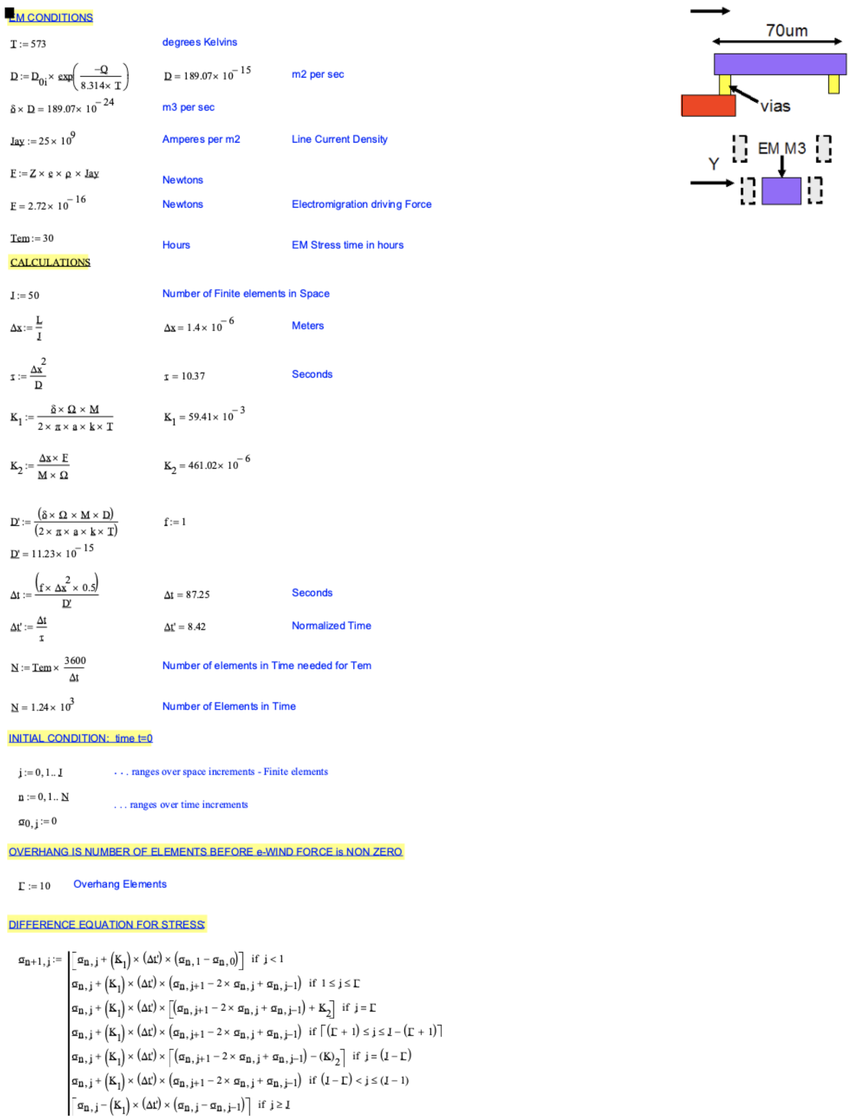

EM CONDITIONS

$T := 573$ degrees Kelvins

$D := D_{0i} \times \exp\left(\frac{-Q}{8.314 \times T}\right)$ $D = 189.07 \times 10^{-15}$ m2 per sec

$\delta \times D = 189.07 \times 10^{-24}$ m3 per sec

$Jay := 25 \times 10^{9}$ Amperes per m2 Line Current Density

$F := Z \times e \times \rho \times Jay$ Newtons

$F = 2.72 \times 10^{-16}$ Newtons Electromigration driving Force

$Tem := 30$ Hours EM Stress time in hours

CALCULATIONS

$I := 50$ Number of Finite elements in Space

$\Delta x := \frac{L}{I}$ $\Delta x = 1.4 \times 10^{-6}$ Meters

$\tau := \frac{\Delta x^2}{D}$ $\tau = 10.37$ Seconds

$K_1 := \frac{\delta \times \Omega \times M}{2 \times \pi \times a \times k \times T}$ $K_1 = 59.41 \times 10^{-3}$

$K_2 := \frac{\Delta x \times F}{M \times \Omega}$ $K_2 = 461.02 \times 10^{-6}$

$D' := \frac{(\delta \times \Omega \times M \times D)}{(2 \times \pi \times a \times k \times T)}$ $f := 1$

$D' = 11.23 \times 10^{-15}$

$\Delta t := \frac{\left(f \times \Delta x^2 \times 0.5\right)}{D'}$ $\Delta t = 87.25$ Seconds

$\Delta t' := \frac{\Delta t}{\tau}$ $\Delta t' = 8.42$ Normalized Time

$N := Tem \times \frac{3600}{\Delta t}$ Number of elements in Time needed for Tem

$N = 1.24 \times 10^{3}$ Number of Elements in Time

INITIAL CONDITION: time t=0

$j := 0, 1 .. I$ . . . ranges over space increments - Finite elements

$n := 0, 1 .. N$ . . . ranges over time increments

$\sigma_{0,j} := 0$

OVERHANG IS NUMBER OF ELEMENTS BEFORE e-WIND FORCE is NON ZERO

$\Gamma := 10$ Overhang Elements

DIFFERENCE EQUATION FOR STRESS:

$$\sigma_{n+1,j} := \begin{cases} \left[\sigma_{n,j} + (K_1) \times (\Delta t') \times (\sigma_{n,1} - \sigma_{n,0})\right] & \text{if } j < 1 \\ \sigma_{n,j} + (K_1) \times (\Delta t') \times (\sigma_{n,j+1} - 2 \times \sigma_{n,j} + \sigma_{n,j-1}) & \text{if } 1 \le j \le \Gamma \\ \sigma_{n,j} + (K_1) \times (\Delta t') \times \left[(\sigma_{n,j+1} - 2 \times \sigma_{n,j} + \sigma_{n,j-1}) + K_2\right] & \text{if } j = \Gamma \\ \sigma_{n,j} + (K_1) \times (\Delta t') \times (\sigma_{n,j+1} - 2 \times \sigma_{n,j} + \sigma_{n,j-1}) & \text{if } \left[(\Gamma + 1) \le j \le I - (\Gamma + 1)\right] \\ \sigma_{n,j} + (K_1) \times (\Delta t') \times \left[(\sigma_{n,j+1} - 2 \times \sigma_{n,j} + \sigma_{n,j-1}) - (K)_2\right] & \text{if } j = (I - \Gamma) \\ \sigma_{n,j} + (K_1) \times (\Delta t') \times (\sigma_{n,j+1} - 2 \times \sigma_{n,j} + \sigma_{n,j-1}) & \text{if } (I - \Gamma) < j \le (I - 1) \\ \left[\sigma_{n,j} - (K_1) \times (\Delta t') \times (\sigma_{n,j} - \sigma_{n,j-1})\right] & \text{if } j \ge I \end{cases}$$

Figure 5.2: MathCAD implementation for stress evolution equation for 300^0C at a current density of 25 mA per square micron and with a overhang size of 3.5 microns for a 70 micron long interconnect.

CHAPTER 6

RESULTS - LINE STRESS

The simulation tool developed in this work using MathCAD was later used for stress estimation for a published experimental electromigration dataset by Vairager et al[4]. Calculations of the stresses were made at the cathode end of typical Cu lines. It has been assumed that mass flow takes place along the line/passivation interface and leads to tension at the cathode end of the line. The most critical unknown quantities are the thickness and diffusivity of the interface.

6.1 Limiting Cases and Test Structure

Two basic limiting cases were studied to place some bounds on the results. For a lower bound estimate of the stress it was assumed that the interface can be treated like a grain boundary in Cu. For an upper bound estimate it was assumed that the interface can be treated like a free surface of Cu. Stress was calculated at the cathode end of a 70 micron Cu line, as shown in Figure 6.1, with the dimensions shown.

The interface thickness was assumed to be 1 nm, probably an upper bound estimate. If surface diffusion is assumed for a Cu line tested at 300^0C and at a current density of 15 mA per square micron then the stress that develops under these conditions is about 270 MPa. If grain boundary diffusion is assumed, the stress is only 25 MPa. These stresses are probably too small to initiate voiding, but of course the conditions that have been used do not lead to

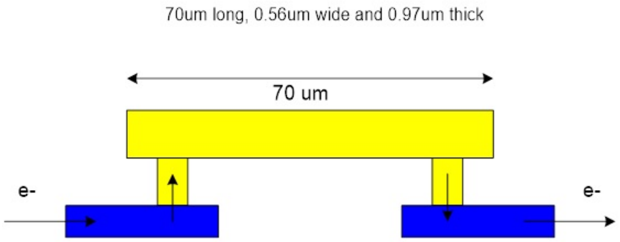

Figure 6.1: Supplied EM test structure

failure.

Stress was calculated at the cathode end of a 70 micron Cu line, using the temperature of 300^0C and current density of 25 mA per square micron. If surface diffusion is assumed at 300^0C and at a current density of 15 mA per square micron then the stress that develops under these conditions is about 770 MPa. If grain boundary diffusion is assumed, the stress is only 80 MPa.

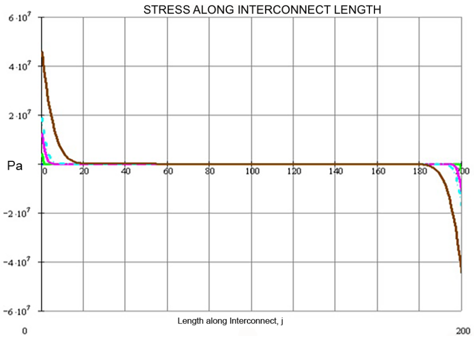

(a) Interface treated like a grain boundary in Cu

(b) interface treated like a free surface of Cu

Figure 6.2: Curves of calculated line stress evolution (at T= 573K and times of 30, 6, 3, 0.3 and 0.03 hours (no change) at a current density of 25 mA per square micron).

6.2 Test Structure Failure Conditions

Conditions for which failure occurred in Intel supplied structures were studied. Intel provided a mean failure time of 330 hours for a Cu line tested at 330^0C and at a current density of 25 mA per square micron. The simulator showed that, assuming that surface diffusion controls the diffusion along the interface, the stress at the end of the line saturates at 770 MPa in about 70 hours (Figure 6.3). This is a very large stress that could surely initiate plastic deformation and eventually failure. Even if grain boundary diffusion is assumed to characterize diffusion along the interface, a large stress of 237 MPa develops in 330 hours. The stresses that develop under the experimental conditions of the in-situ EM experiments are much less, consistent with the fact that failure does not occur under these conditions. It is encouraging that these simulations not only provided a useful guide to the experiments but have also proven useful in connecting the numerical results to the observed plasticity and eventual failure of the interconnect line.

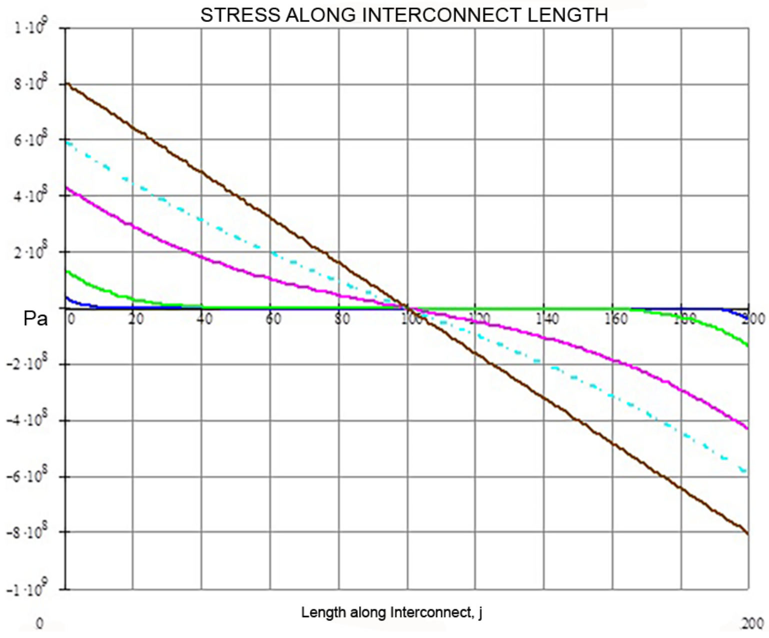

Figure 6.3: Curves of calculated stress evolution for the supplied test structure (at T= 603K and times of 70, 14, 7, 0.7 and 0.07 hours (no change) at a current density of 25 mA per square micron and the interface treated like a free surface of Cu

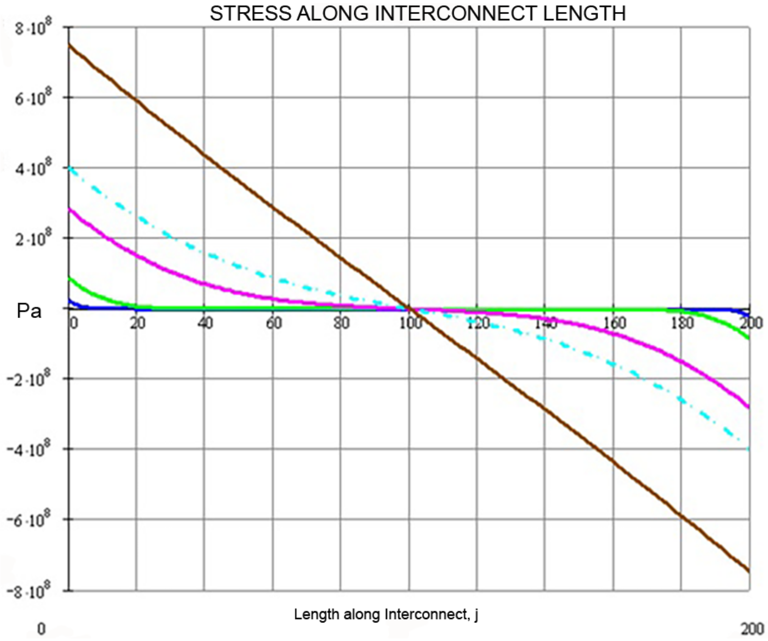

Figure 6.4: Curves of calculated stress evolution in an interconnect line (at T= 573K and times of 30, 6, 3, 0.3 and 0.03 hours (no change) at a current density of 25 mA per square micron). The interface is treated like a free surface of Cu and the interconnect has no overhang length. Peak stress reached is 750 MPa.

6.3 Effect of Overhang

Stress evolution curves were simulated for a line with no overhang (Figure 6.4) and also for the case where the line was assumed to have ten finite difference elements as overhangs on each side of the vias (Figure 6.5). This amounts to an overhang length of 3.5 microns for an interconnect length of 70 microns. The effect of the overhang is to reduce the tensile and compressive stresses at the ends of the interconnect. The stress reaches a peak value where the overhang overlaps with the via element (Figure 6.5). The simulation also suggests that it takes longer, under the same stress conditions, to reach a particular stress value. The advantage of this becomes clear when failure occurs at a critical stress. In general, it would take longer to reach critical failure stress conditions with some amount of overhang (reservoir). As explained earlier, the effect of the reservoir is to improve the electromigration lifetime.

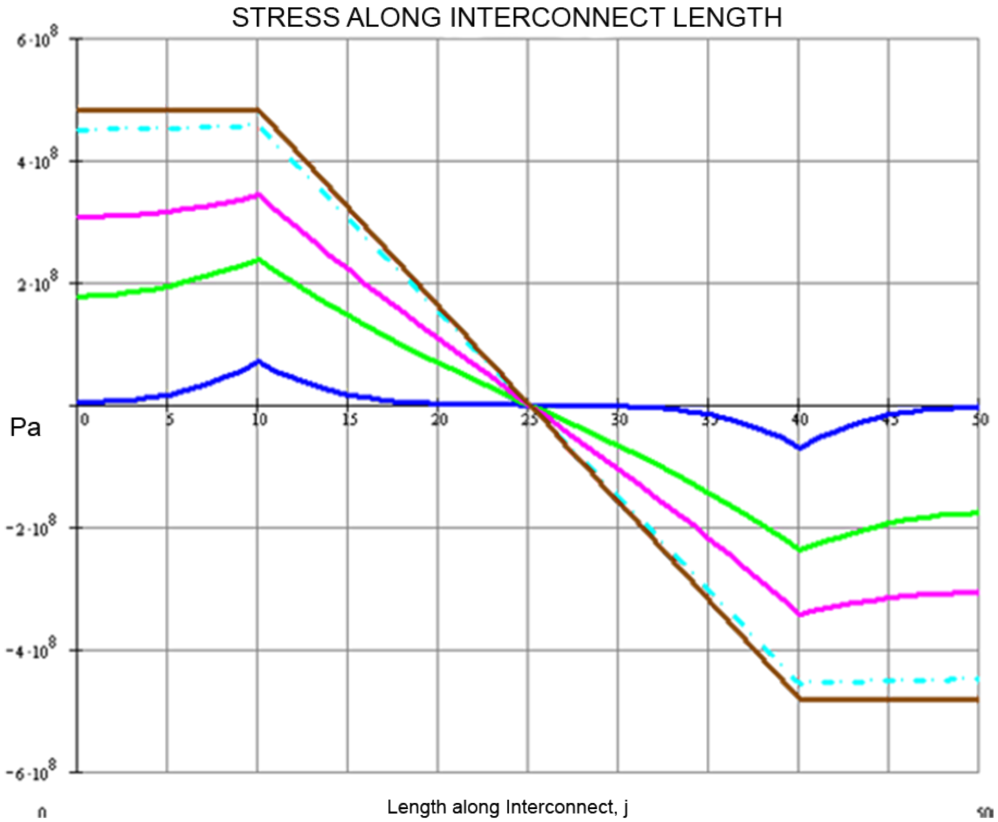

Figure 6.5: Curves of calculated stress evolution in an interconnect line (at T= 573K and times of 30, 6, 3, 0.3 and 0.03 hours (no change) at a current density of 25 mA per square micron). The interface is treated like a free surface of Cu and the interconnect has a overhang length of 3.5 microns at the ends. Peak stress reached is 450 MPa.

6.4 Line Stress Conclusions

A one dimensional model for electromigration induced stress evolution has been developed. Numerical implementation was performed using the method of finite differences. A MathCAD tool was developed to realize the numerical implementation.

Two basic limiting cases were studied to place some bounds on the results. For a lower bound estimate of the stress it was assumed that the interface can be treated like a grain boundary in Cu. For an upper bound estimate it was assumed that the interface can be treated like a free surface of Cu. Measured failure times and known structure geometries for experimental samples were used to estimate the stress build-up in the interconnect lines.

Line stress build-up for interconnect structures with overhang elements were simulated using the developed tool. Results show that the advantage of the overhangs is to improve the electromigration lifetime of interconnect lines by reducing the time taken to reach peak stress. The stress is at the peak value over the vias.

The model developed needs further work by taking into account, the vacancy flows into the crystal in the vertical direction.

CHAPTER 7

COMPARISON OF EXPERIMENTAL AND SIMULATION DATA

Existing electromigration Time to Fail (TTF) data from studies conducted and published by Vairagar et al[4] was used to compare existing experimental electromigration data with our simulated stress data for similar test structures. Electromigration TTF Data was available for experimental samples with known structure geometries and test conditions. Calculated line stress was compared with available TTF data for the interconnect lines. TTF to line stress correlation was investigated for various sample geometries and test conditions.

7.1 Results

Simulation runs were performed using the developed numerical scheme using MathCAD. Stress calculations were simulated for units with known geometry, electromigration stress conditions and TTF (Table 7.1). For the calculations it was assumed that the interface can be treated like a free surface of Cu.

7.2 Effect of Geometry and Temperature on Line Stress

For the narrow geometry samples stressed at the same current density, the calculated line stress at TTF is independent of electromigration temperature. Wider geometry units also show a similar trend in line stress build up that does not vary with temperature for a particular stress current density. However, compared to the narrow units, the line stress at TTF is much lower for the wider units for electromigration under similar conditions. One explanation for the lower simulated line stress build up at TTF for the wider units could be that wider units undergo a much larger mass transport in less time when compared to the narrow units and therefore the line stress levels need not build up to the same levels at TTF.

7.3 Effect of Geometry and Current Density on Line Stress

For a fixed geometry and temperature, higher electromigration current densities result in lower TTF, as expected, but the calculated line stress at TTF is higher for higher electromigration current densities. However, compared to the narrow geometry samples, the line stress at TTF is again lower for wider units with the same electromigration temperature and current densities. Although we can explain the lower stress for wider lines by making the mass transport argument again, it is not readily clear as to why the stress at TTF is higher for higher electromigration current densities and with fixed geometry and temperature. More analysis is needed. The effect of geometry, temperature and current density on line stress is summarized in Table 7.2.

Table 7.1: Line stress calculations for units with known geometries, test conditions and TTF data

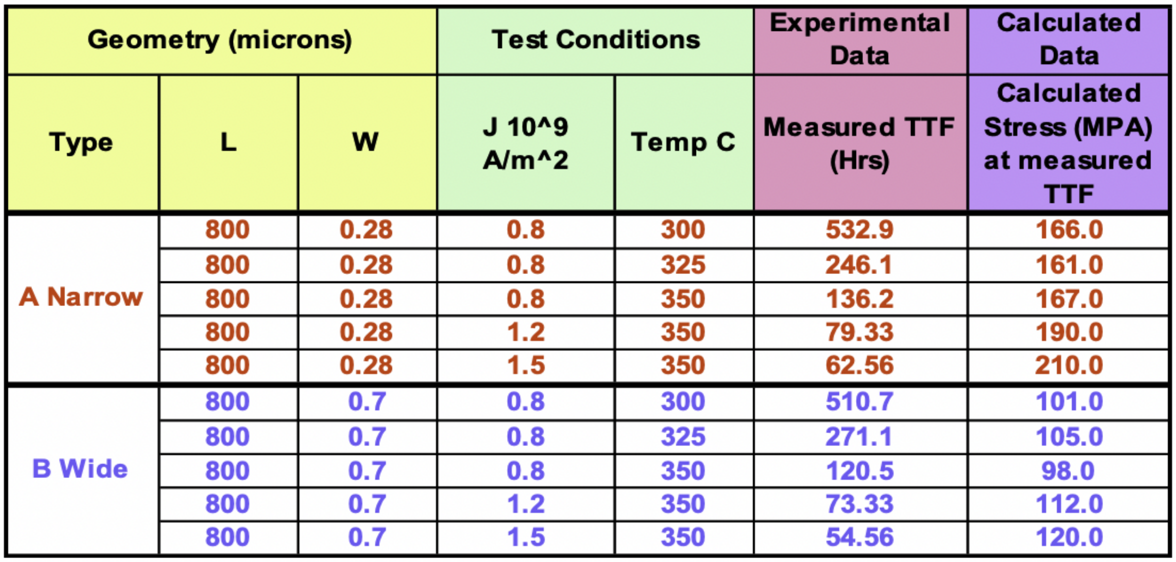

Geometry (microns)			Test Conditions		Experimental Data	Calculated Data
Type	L	W	J 10^9 A/m^2	Temp C	Measured TTF (Hrs)	Calculated Stress (MPA) at measured TTF
A Narrow	800	0.28	0.8	300	532.9	166.0
	800	0.28	0.8	325	246.1	161.0
	800	0.28	0.8	350	136.2	167.0
	800	0.28	1.2	350	79.33	190.0
	800	0.28	1.5	350	62.56	210.0
B Wide	800	0.7	0.8	300	510.7	101.0
	800	0.7	0.8	325	271.1	105.0
	800	0.7	0.8	350	120.5	98.0
	800	0.7	1.2	350	73.33	112.0
	800	0.7	1.5	350	54.56	120.0

Table 7.2: The effect of geometry, temperature and current density on line stress

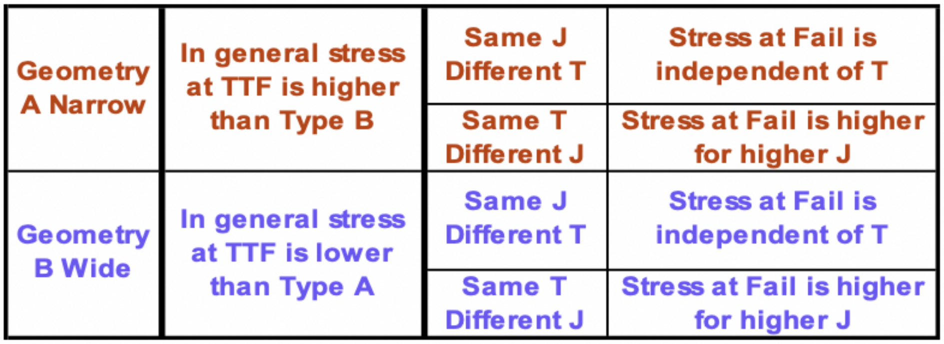

Geometry A Narrow	In general stress at TTF is higher than Type B	Same J Different T	Stress at Fail is independent of T
		Same T Different J	Stress at Fail is higher for higher J
Geometry B Wide	In general stress at TTF is lower than Type A	Same J Different T	Stress at Fail is independent of T
		Same T Different J	Stress at Fail is higher for higher J

7.4 Experimental vs Simulation Data Conclusions

In this work we investigated the correlation of measured electromigration TTF with calculated line stress. Line stress models are physically based, in contrast to the empirically based Black's law. If EM TTF correlates with line stress, we have a means for predicting line TTF thru stress calculations.

In general, for particular line geometry, the calculated line stress at TTF is constant and independent of electromigration temperature and furthermore line stress levels at TTF seem to go down for wider geometries. Line stress at TTF is higher for higher electromigration current densities and with fixed geometry and temperature. Further investigation is needed to understand the effect of current density on line stress. This is presented in the subsequent chapter on current crowding.

CHAPTER 8

MOLECULAR DYNAMICS

Molecular Dynamics (MD) is a simulation technique[7] for complex material systems, modelled at the atomic level. The equations of motion are solved numerically to follow the time evolution of the system, allowing the derivation of kinetic and thermodynamic properties of interest.

In MD simulations the time evolution of a set of interacting particles is calculated via the solution of Newton's equations of motion, as shown in Equation 8.1, where $r_i(t) = (x_i(t), y_i(t), z_i(t))$ is the position vector of ith particle and F_i is the force acting upon ith particle at time t and m_i is the mass of the particle.

$$F_i = m_i \frac{\partial^2 r_i(t))}{\partial t^2} \tag{8.1}$$

The particles usually correspond to atoms and may represent any distinct entities that can be conveniently described in terms of a certain interaction law. To integrate the above second order differential equations the instantaneous forces acting on the particles and their initial positions and velocities must be specified. Due to the multiple body nature of the problem the equations of motion are solved numerically. The calculated trajectories are defined by both position and velocity vectors and describe the time evolution of the system in space within a finite time interval.

8.1 Modeling of Electromigration Using Molecular Dynamics Simulations

The modeling of thermal transport in solids at non-equilibrium conditions is popular using classical Molecular Dynamics (MD), which has the advantage of explicitly representing phonon modes and the scatterers of phonons, such as defects and boundaries. However, the disadvantage of MD is the missing ability for modeling free electrons and their role in thermal transport. These electronic effects are vital in the performance of electronic devices in general and therefore present significant challenges to model Electromigration using Molecular Dynamics, in general[30].

As a first cut attempt to model Electromigration in MD simulations[31], an extra force was added on each atom in a lattice and the total force F_{Total} calculated at each time step as a sum of F_{EAM} and F_{EM} where F_{EAM} is the force calculated by Embedded-Atom-Method (EAM) and F_{EM} is the force due to electron atom interactions triggered by collisions and momentum transfer.

$$F_{Total} = F_{EAM} + F_{EM} \tag{8.2}$$

8.2 Molecular Dynamics Implementation of EM using LAMMPS Software

LAMMPS[8] is a classical Molecular Dynamics code written in C++ programming language that can model an ensemble of particles in a liquid, solid, or gaseous state. It can model metallic, granular, and coarse-grained systems using a variety of force fields and boundary conditions. LAMMPS integrates Newton's equations of motion for collections of atoms, molecules, or macroscopic particles that interact via short or long-range forces with a variety of initial or boundary conditions.

In this work, electromigration has been implemented as a two step process using LAMMPS. Some prior work involving LAMMPS for Silver electromigration was performed by Xu and Hook et al [32]. The first step relaxes a specified and finite block of Copper conductor model at 1000K. LAMMPS code runs output a visualization file. Since all atoms are initially created in a perfect Face centered cubic (FCC) lattice position with a lattice constant of 0.3597nm, the Cu system needs relaxation to reach a stable status at the simulation temperature. A void was introduced in the lattice in order to create an imperfection that would help with simulated diffusion as an otherwise perfect crystal has no such vacancies to help with the diffusion process. No extra force F_{EM} was added at this stage of relaxation simulation for a period of 0.5ns. In the following 0.1ns, F_{EM} was ramped from 0 to 16pN (pico Newtons) and at a constant rate and it was maintained so until the end of the simulation. The timestep was 1fs.

The thermal effect of the current was neglected and a thermostatic ensemble was used. In order to prevent the system from moving freely as a whole when extra force was added, an edge of the block system was fixed (shrink wrapped) after system relaxation. The extra force is similar to the electron wind force F_{EM}.

Figures 8.1 and 8.2 show the LAMMPS code used for Cu block relaxation at 1000K and it Visualization using Visual Molecular Dynamics (VMD) software [33][34], respectively.

Figures 8.3 to 8.7 show the Visualization of LAMMPS specified finite Cu Block after relaxation at 1000K and 0.5ns. The visualization in the figures illustrate the movement of atoms under the influence of an electron wind force, as simulated. Some atoms are marked and color coded for tracking purpose. The marking does not influence the force on these atoms.

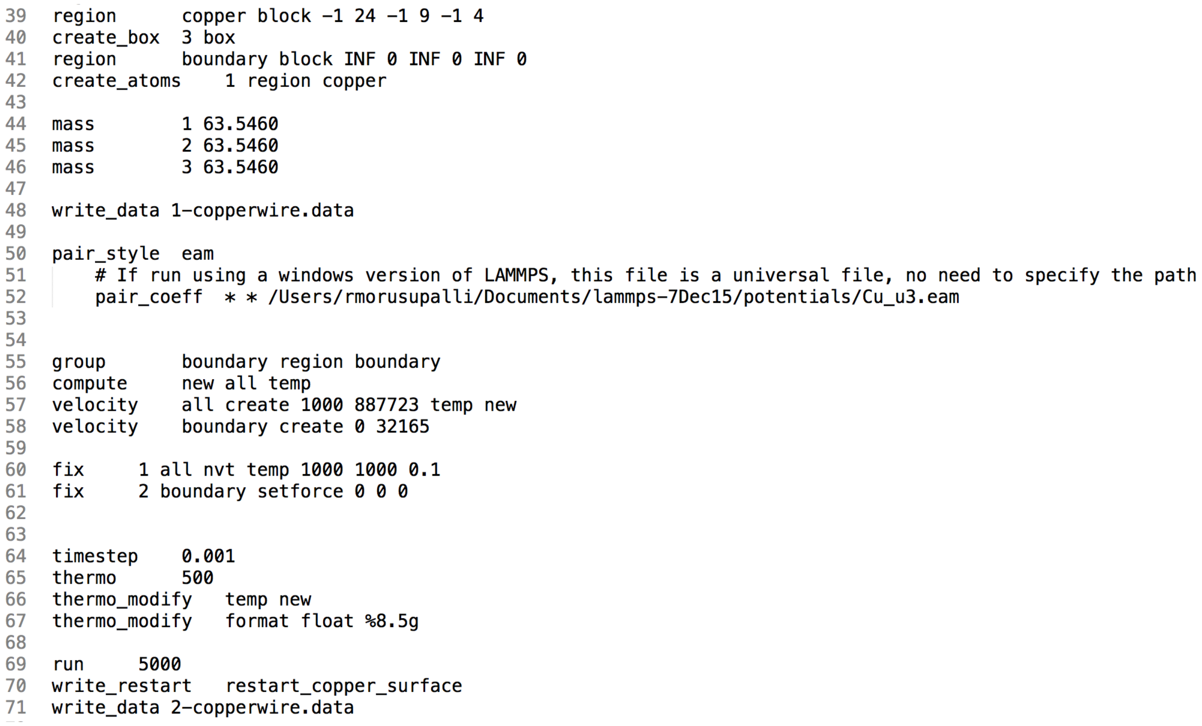

```
region      copper block -1 24 -1 9 -1 4
create_box  3 box
region      boundary block INF 0 INF 0 INF 0
create_atoms    1 region copper

mass        1 63.5460
mass        2 63.5460
mass        3 63.5460

write_data 1-copperwire.data

pair_style  eam
    # If run using a windows version of LAMMPS, this file is a universal file, no need to specify the path
    pair_coeff  * * /Users/rmorusupalli/Documents/lammps-7Dec15/potentials/Cu_u3.eam


group       boundary region boundary
compute     new all temp
velocity    all create 1000 887723 temp new
velocity    boundary create 0 32165

fix     1 all nvt temp 1000 1000 0.1
fix     2 boundary setforce 0 0 0


timestep    0.001
thermo      500
thermo_modify   temp new
thermo_modify   format float %8.5g

run     5000
write_restart   restart_copper_surface
write_data 2-copperwire.data
```

Figure 8.1: Step 1: LAMMPS code for Cu Block relaxation at 1000K

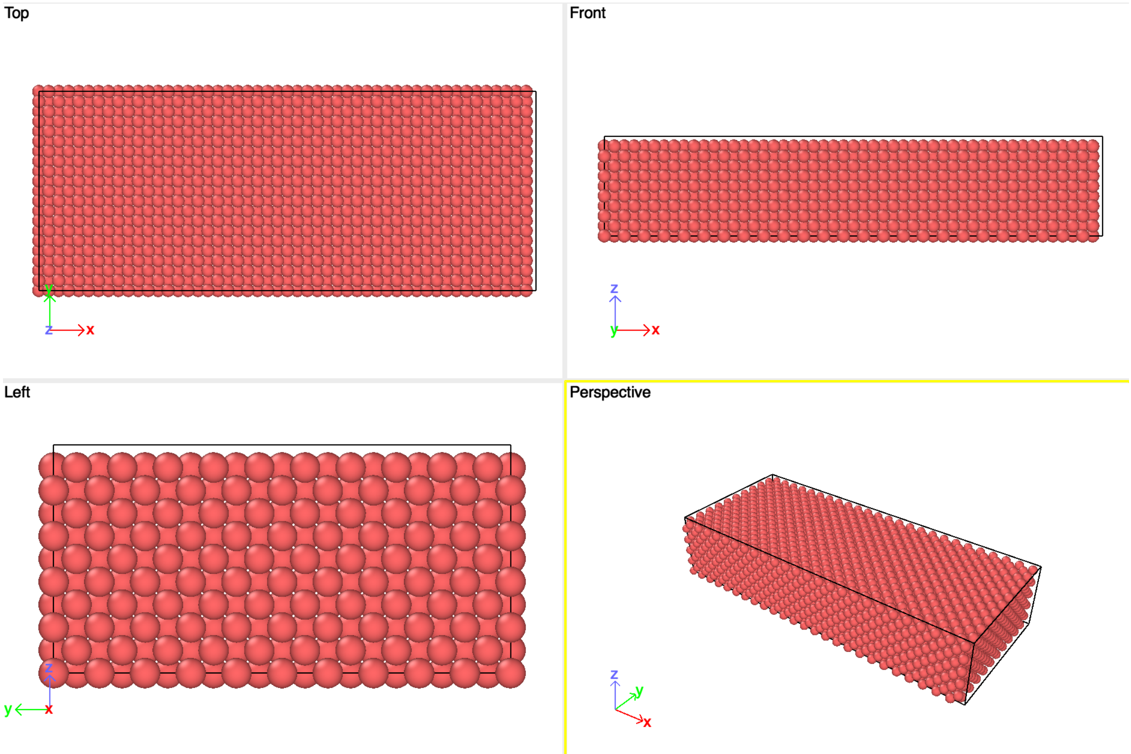

Figure 8.2: Visualization of LAMMPS Specified finite Cu Block before relaxation

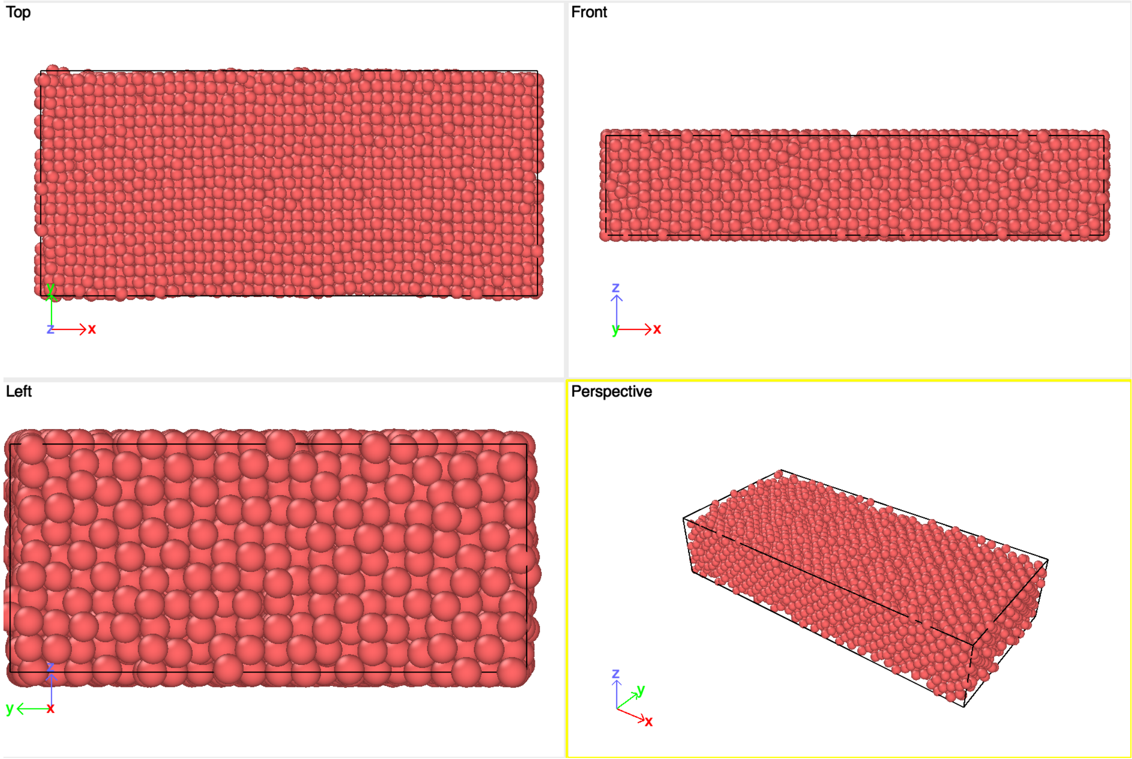

Figure 8.3: Visualization of LAMMPS Specified finite Cu Block after relaxation at 1000K and 0.5ns

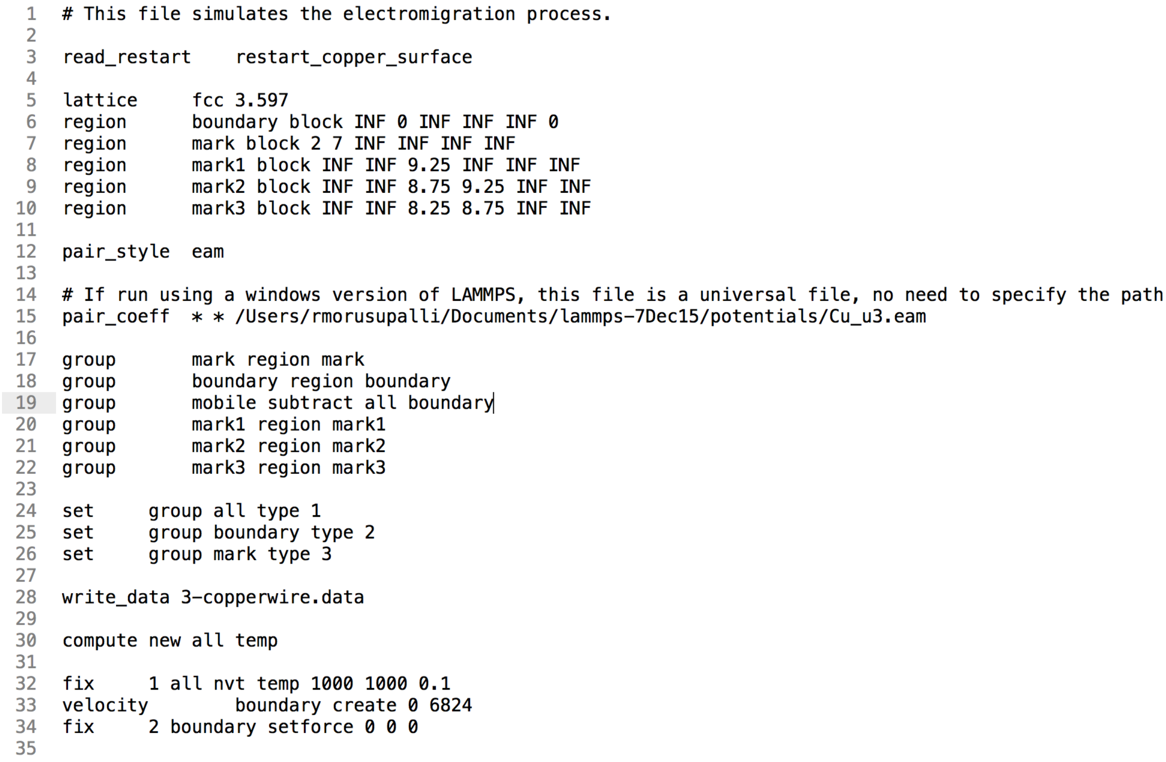

```
# This file simulates the electromigration process.

read_restart    restart_copper_surface

lattice     fcc 3.597
region      boundary block INF 0 INF INF INF 0
region      mark block 2 7 INF INF INF INF
region      mark1 block INF INF 9.25 INF INF INF
region      mark2 block INF INF 8.75 9.25 INF INF
region      mark3 block INF INF 8.25 8.75 INF INF

pair_style  eam

# If run using a windows version of LAMMPS, this file is a universal file, no need to specify the path
pair_coeff  * * /Users/rmorusupalli/Documents/lammps-7Dec15/potentials/Cu_u3.eam

group       mark region mark
group       boundary region boundary
group       mobile subtract all boundary
group       mark1 region mark1
group       mark2 region mark2
group       mark3 region mark3

set     group all type 1
set     group boundary type 2
set     group mark type 3

write_data 3-copperwire.data

compute new all temp

fix     1 all nvt temp 1000 1000 0.1
velocity        boundary create 0 6824
fix     2 boundary setforce 0 0 0

```

Figure 8.4: Step 2: LAMMPS code for Cu Electromigration Simulation

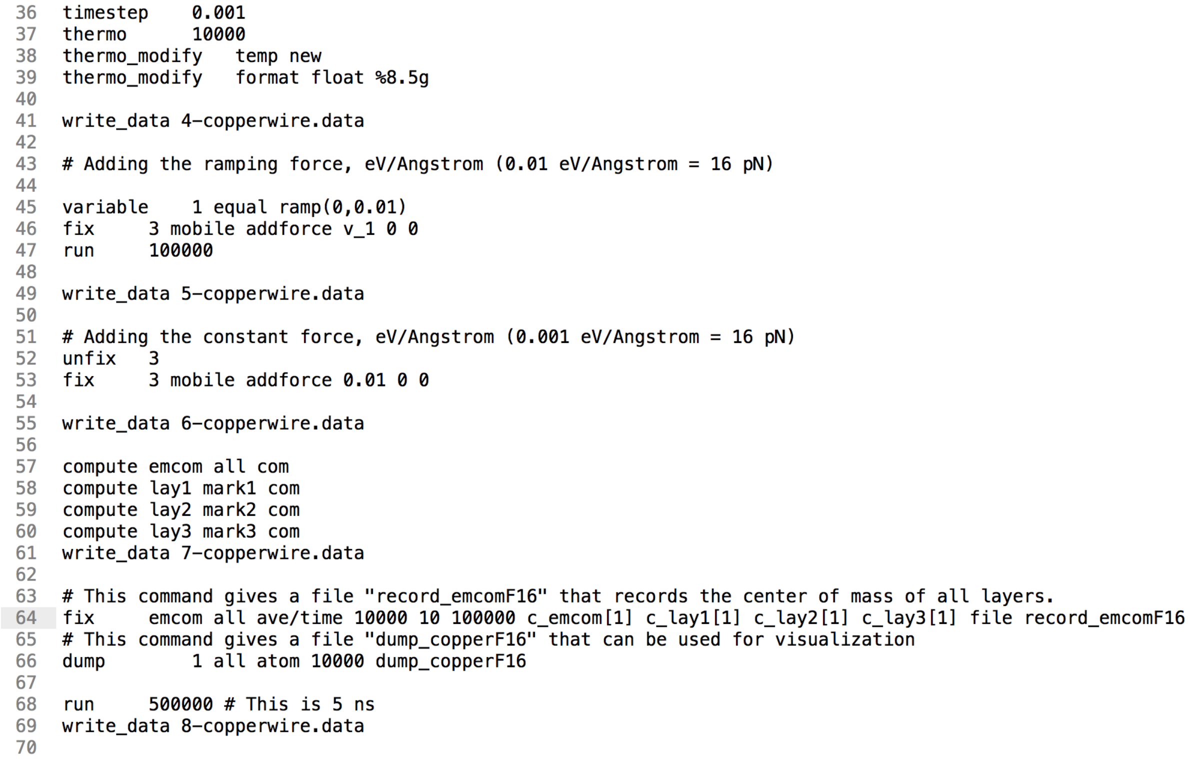

```
timestep    0.001
thermo      10000
thermo_modify   temp new
thermo_modify   format float %8.5g

write_data 4-copperwire.data

# Adding the ramping force, eV/Angstrom (0.01 eV/Angstrom = 16 pN)

variable    1 equal ramp(0,0.01)
fix     3 mobile addforce v_1 0 0
run     100000

write_data 5-copperwire.data

# Adding the constant force, eV/Angstrom (0.001 eV/Angstrom = 16 pN)
unfix   3
fix     3 mobile addforce 0.01 0 0

write_data 6-copperwire.data

compute emcom all com
compute lay1 mark1 com
compute lay2 mark2 com
compute lay3 mark3 com
write_data 7-copperwire.data

# This command gives a file "record_emcomF16" that records the center of mass of all layers.
fix     emcom all ave/time 10000 10 100000 c_emcom[1] c_lay1[1] c_lay2[1] c_lay3[1] file record_emcomF16
# This command gives a file "dump_copperF16" that can be used for visualization
dump        1 all atom 10000 dump_copperF16

run     500000 # This is 5 ns
write_data 8-copperwire.data

```

Figure 8.5: Continuation of Step 2: LAMMPS code for Cu Electromigration Simulation

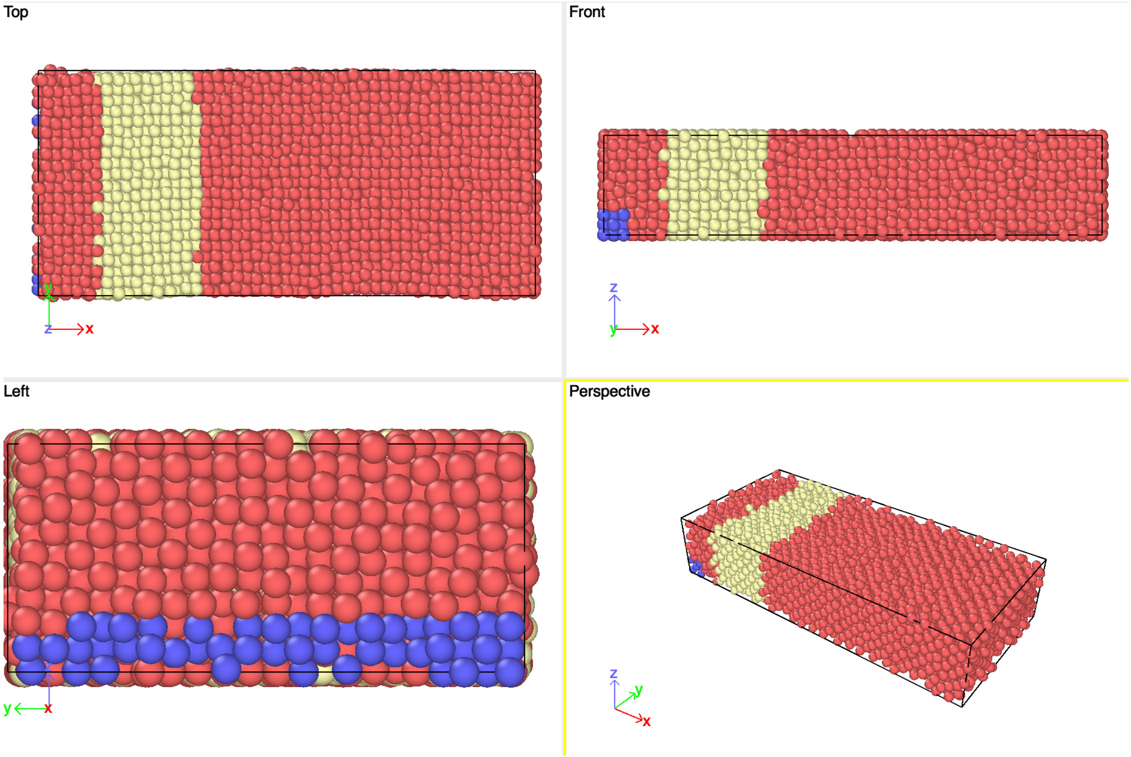

Figure 8.6: Visualization of LAMMPS Specified finite Cu Block before Electromigration simulation. A strip of atoms were marked blue (surface) and yellow (bulk) to monitor the movement of atoms. The marking does not influence the force on these atoms.

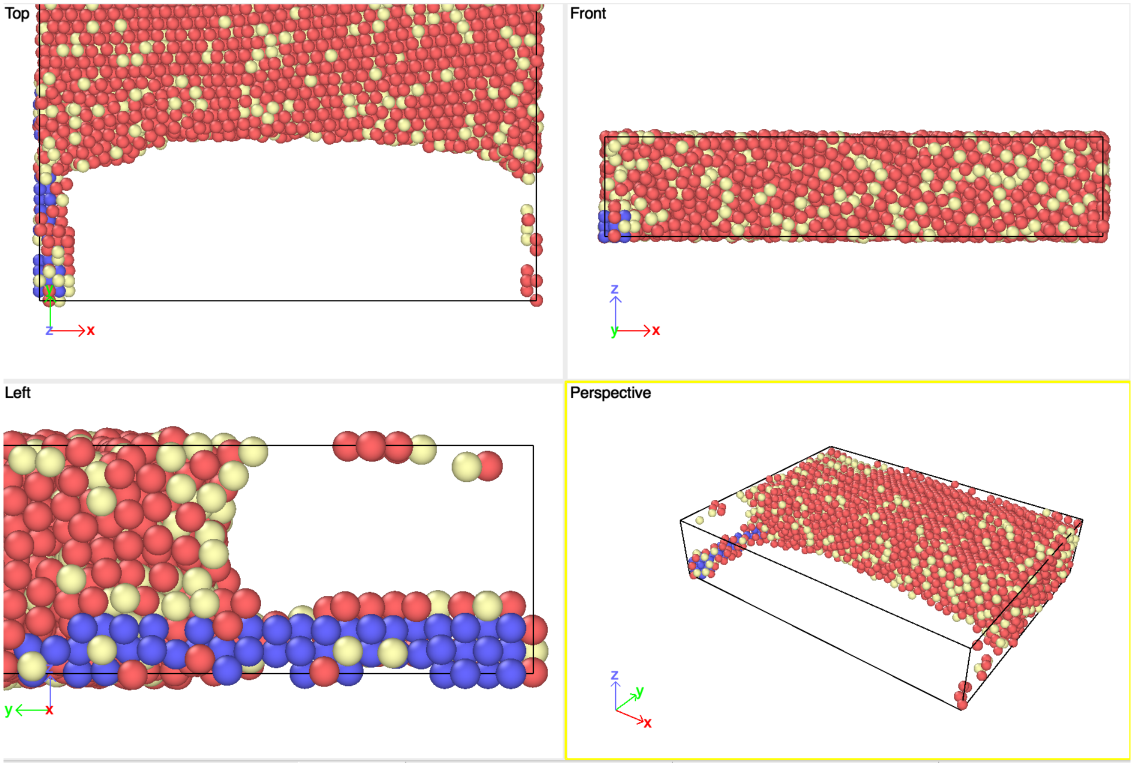

Figure 8.7: Visualization of LAMMPS Specified finite Cu Block after Electromigration simulation.

8.3 Next Steps for Simulation Work

LAMMPS software is very advanced with many applications, however, based on the attempts performed in this work, it is probably not very suitable for simulation of electron and thermal transport. Although we could successfully superimpose a force to simulate an electron wind force using LAMMPS, methods for further simulation work were not achieved. We have therefore not obtained any significant results using LAMMPS for simulation of electromigration. No further simulation work using LAMMPS was completed, however, intent was to apply one dimensional models using more suitable simulation tools such as MATLAB by incorporating electron flow and thermal transport in electromigration. Such simulation work was used to characterize the effect of current crowding on line stress evolution. This is presented in a later chapter of this work.

CHAPTER 9

EFFECT OF MAGNETIC FIELDS ON ELECTROMIGRATION

Magnetic fields can be produced by electric currents (moving charges), which can be macroscopic currents as in conducting metal wires or microscopic currents associated with moving electrons in atomic orbits. Geometries that enhance current crowding can also impact such magnetic fields within the conductor. Of particular interest is the high density current flows in the interconnects of an integrated circuit and the effect such currents have in creating their own magnetic fields and their impact on migrating lattice ions.

9.1 Link between Electric Currents and Magnetic Fields

In 1820, Hans Christian Oersted[35] discovered that a current carrying wire deflects a nearby compass by exerting a force on its magnetic needle. Neglecting the earth's magnetic field, the compass needle always aligns in a direction perpendicular to the current carrying wire. This was the first experiment to establish a link between electricity and magnetism which until then were treated as distinct and unrelated phenomena. Just as an electric current (a moving charge) produces a magnetic field, a charge that is moving under the influence of a magnetic field will experience a magnetic force on itself due to its charge and motion.

9.2 The Biot-Savart Law and the Lorentz Force

In order to analyze the impact of magnetic fields in the context of electromigration we start by looking at the forces on a lattice atom due to the magnetic field induced upon them by moving electrons elsewhere in the same conductor, followed by an analysis which looks at what a force such as this might do to the net diffusion path of these lattice atoms undergoing Electromigration, noting that a path adopted by a diffusing lattice atom leaves behind a migrating void in some other direction.

Biot-Savart law[36] gives the magnetic field due to an infinitesimal length “dl”, the current element, of a larger current carrying conductor. The total magnetic field at a point in space that is at a perpendicular distance “R” from the current carrying line can then be found by integrating over the total length of all such current elements:

$$d\mathbf{B} = \frac{\mu_0}{4\pi}\frac{Id\ell \times \hat{\mathbf{r}}}{r^2} \tag{9.1}$$

The current “I” shown in the diagram is the conventional current representing flow of positive charges and the direction of electron flow is therefore opposite to the direction of “I” as indicated. The total magnetic field at the point is then obtained by integrating the field due to each current element as follows.

$$\mathbf{B} = \frac{\mu_\mathbf{0}}{\mathbf{4}\pi}\int \frac{\mathbf{Id}\ell \times \hat{\mathbf{r}}}{\mathbf{r^2}} \tag{9.2}$$

It can be shown further (after evaluating the integral) that the magnetic field can be expressed as:

$$\mathbf{B} = \frac{\mu_0 \mathbf{I}}{2\pi \mathbf{R}} \tag{9.3}$$

In order for a force to be exerted on a charge “q” (at this point) due to the magnetic field, the charge must be in motion because the magnetic force on a stationary charge or on a charge moving parallel to the magnetic field is always zero. Force on the point with charge “q” and moving with a velocity “v” is given by the cross product:

$$F = q\mathbf{v} \times \mathbf{B} \tag{9.4}$$

This is the Lorentz force on a moving charge due to magnetic the field. The direction of the force can be determined using the right hand rule as illustrated in Figure 9.1. The force is always perpendicular to the direction of motion and the direction of the magnetic field.

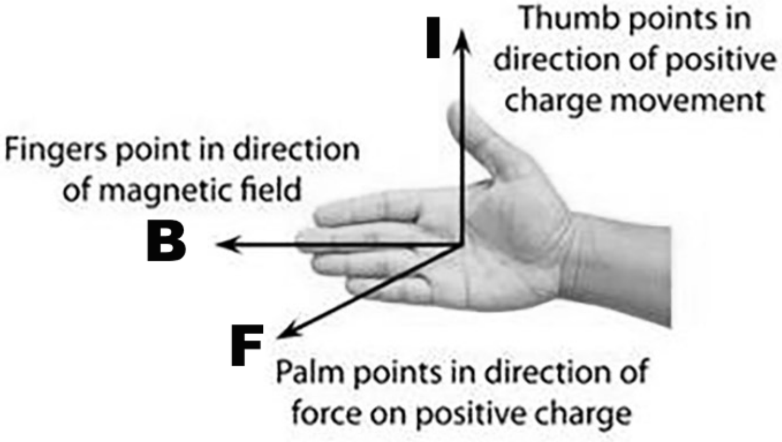

Figure 9.1: Right hand rule. Given the direction of the conventional current I, the curl of the fingers determines the direction of the magnetic field B and the palm of the right hand determines the direction of the force on the flowing positive charge.

9.3 Source of the Magnetic Field during Electromigration

In this work the magnetic field produced by moving electrons, an electric current, and its effect on lattice atoms, particularly the force exerted on moving lattice atoms that may be undergoing a slow but steady movement in the direction of the electron flow (ie a steady state Electromigration) is investigated. Literature survey shows very little research by groups in academia or industry. Although there has been some prior work to be found in the study of Magnetomechanical instabilities in materials [37] [38] there is very limited to no prior research into the effects of magnetic fields and Lorentz forces on atomic flux during electromigration.

A note on “moving lattice atoms” as referenced here: The lattice atoms are fixed, unlike the moving electrons, however they are never really at absolute rest state not only due to intrinsic thermal vibrations but also because in a system that is undergoing Electromigration, the lattice atoms are known to undergo a net force that tends to move the atoms in a general direction that is from the anode to cathode end of the interconnect.

In a conductor with electrons flowing in a positive x direction, lattice ions also migrate in the direction of electron flow. The flowing electrons generate a magnetic field in the negative z direction and a positively charged migrating lattice ion will experience a Lorentz force in the negative y direction. This is easy to visualize using the right hand rule. The question that must be asked is whether or not this magnetic field results in a sufficient magnitude and direction of the Lorentz force that may result in either aiding or inhibiting the process of electromigration and/or void formation. An estimation of relative magnitudes of the electron wind and Lorentz forces is presented in the following section.

9.4 Estimation of the Lorentz Force

Current density in an interconnect line would produce not only electron wind forces but also Lorentz forces on a lattice ion migrating in the direction of electron flow and under the influence of a magnetic field. An estimation of the magnitude of the Lorentz forces compared to the electron wind forces for a simple geometry has been calculated in this section. Such an estimate for a simple geometry of an interconnect line would produce useful insights.

Consider an interconnect line of width $w = 2a$ and thickness t carrying a current I which is uniformly distributed over the cross-section of the line as shown in the Figure 9.2.

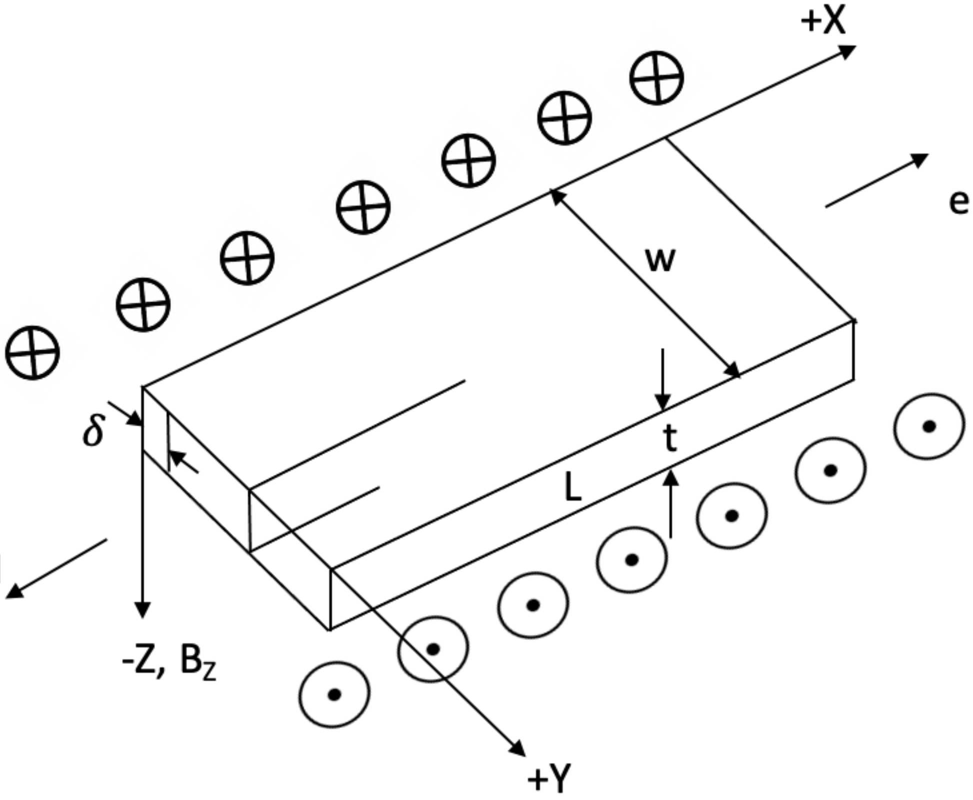

Figure 9.2: Interconnect line of width $w = 2a$ and thickness t carrying a current I which is uniformly distributed over the cross-section of the line

The electron wind force acting on a positive ion is known to be:

$$F_x{}^e = -eZ^*\rho j \tag{9.5}$$

where eZ^* is the effective change on the ions, ρ is the resistivity of the metal line and J is the current density[28].

The dimensions of the terms in this relation are:
$-eZ^*$: C ($Coulombs$),
ρ: $Volt\ m/A$,
J: A/m^2 and
$F_x{}^e$: $Newtons$

For ions located a small distance δ from the edge of the line and drifting in response to the electron wind there, a Lorentz force of:

$$F_y{}^B = -qvB_z \tag{9.6}$$

acts on the ions, where q is the charge on the ions, v is the drift velocity (in the x direction) and B_z is the magnetic field at $y = \delta$ due to the current elsewhere in the line. The dimensions of the terms in this relation are: q: C ($Coulombs$), v: m/s, B_z: T (Tesla or $Newton$ / Am) and the force $F_y{}^B$ has the dimensions of $Newtons$.

To determine $F_y{}^B$ we need to calculate B_z at $y = \delta$ using the Biot-Savart law for the magnetic field associated with a current. The current flowing in the domain from y to $y + dy$, i.e. dI, produces a magnetic field dB_z at $y = \delta$ given by:

$$\mathbf{dB_z} = \frac{\mu_0 \mathbf{dI}}{\mathbf{2}\pi(\mathbf{y}-\delta)}$$

$$d\mathbf{I} = \mathbf{J}.\mathbf{dy}.\mathbf{t}$$

where μ_0 is the permeability. For free space the permeability μ_0 is equal to $4\pi 10^{-7}\ Tm/A$

One can see that $\mathbf{dB_z}$ is singular as $y \to \delta$, so we should calculate $\mathbf{dB_z}$ from $y = 2\delta$ to $y = W$.

$$B_z(y=\delta) = \int_{2\delta}^{W} d\mathbf{B_z} = \int_{\mathbf{2}\delta}^{\mathbf{W}} \frac{\mu_0 \mathbf{Jt}}{\mathbf{2}\pi(\mathbf{y}-\delta)}\mathbf{dy}$$

$$B_z(y=\delta) = \frac{\mu_0 Jt}{2\pi}\int_{2\delta}^{W}\frac{dy}{(y-\delta)}$$

$$= \frac{\mu_0 Jt}{2\pi}\ln(y-\delta)\binom{W}{\delta}$$

$$= \frac{\mu_0 Jt}{2\pi}[(\ln(W-\delta) - \ln(2\delta-\delta)]$$

$$B_z(y=\delta) = \frac{\mu_0 Jt}{2\pi}\ln(\frac{W-\delta}{\delta}) \tag{9.7}$$

Now consider the magnetic field associated with the current in the domains $0 < y < \delta$ and $\delta < y < 2\delta$. The magnetic fields from the currents in these two domains will cancel exactly so the above result for $B_z(y=\delta)$ should be correct. Obviously as $\delta \to 0$ $B_z \to \infty$.

The drift velocity of the ions, v can be expressed as:

$$v = M{F_x}^e \tag{9.8}$$

where M is the mobility of the ion.

Using this velocity with Equation (9.6) and using Equation (9.7) to get B_z we have:

$$ {F_y}^B = -qM{F_x}^e \frac{\mu_0 Jt}{2\pi} \ln(\frac{W-\delta}{\delta}) \tag{9.9}$$

Now we can calculate the magnitude of ${F_y}^B$, i.e. $\left|{F_y}^B\right|$ and compare it with the magnitude of ${F_x}^e$, $|{F_x}^e|$,

$$\left|\frac{{F_y}^B}{{F_x}^e}\right| = qM \frac{\mu_0 Jt}{2\pi} \ln(\frac{W-\delta}{\delta}) \tag{9.10}$$

We see that if the ions are immobile, the mobility $M = 0$, as expected. Also, the magnitude of ${F_y}^B$ depends on the current density and the thickness of the line.

The dimensions of $\left|\frac{{F_y}^B}{{F_x}^e}\right| = dimensionless$. To estimate the magnitude of ${F_y}^B$ compared to F_x^e let's take the mobility of the ions using Einstein's simple mobility law:

$$M = \frac{D}{kT} \tag{9.11}$$

and using Equation 9.8 the velocity can be easily shown to be:

$$v = \frac{D}{kT}F \tag{9.12}$$

Using Equation 9.11 and substituting for mobility M in Equation 9.10, the ratio of the forces can be written as:

$$\left| \frac{{F_y}^B}{{F_x}^e} \right| = q\frac{D}{kT}\frac{\mu_0 Jt}{2\pi}\ln(\frac{W-\delta}{\delta}) \tag{9.13}$$

where D is the diffusion coefficient for the ions and given by:

$$D = D_o \exp\frac{-Q}{kT}$$

To make an estimate of the ratio we will consider bulk diffusion in Aluminum by assuming the following values:

$D_0 = 2.25 \times 10^{-4}\,\frac{m^2}{S}$ and $Q = 1.5eV$

To take an extreme case, consider $T = 500°C$ or $T = 773°K$.

$k = 8.63 \times 10^{-5}\frac{eV}{K}$

$kT = 8.63 \times 10^{-5} \times 773 = 6.67 \times 10^{-2}$

so $D = 2.25 \times 10^{-4} \exp\frac{-1.5}{6.67\times10^{-2}}$

$D = 4.18 \times 10^{-14}\,\frac{m^2}{s}$

$kT = 1.38 \times 10^{-23} \times 773 = 1.066 \times 10^{-20}\,J$

So the mobility would be:

$M = \frac{D}{kT} = \frac{4.18\times10^{-4}\,(m^2/s)}{1.066\times10^{-20}\,(J)}$

$M = 3.92 \times 10^{16}\,\frac{m}{Ns}$

The charge on a singly charged migrating ion might can be assumed to be $1.6 \times 10^{-19}C$

Let's also take the current density to be:

$10\frac{mA}{(\mu m)^2} = 10\frac{A}{(m)^2}$

$J = 10^{10}\,\frac{A}{m^2}$

and the thickness of the line is assumed to be $t = 0.1\,\mu m = 10^{-7}\,m$

and the width of the line is assumed to be $W = 1\,\mu m = 10^{-6}\,m$

and the distance to the edge of the line is assumed to be $\delta = 0.1\,\mu m = 10^{-7}\,m$

Therefore:

$$\left|\frac{F_y{}^B}{F_x{}^e}\right| = (1.6\times10^{-19})\times(3.92)\times10^{16}\times(4\pi\times10^{-7}\times(10^{10})\times(10^{-7})\times\frac{1}{2\pi}\ln(\frac{1-0.1}{0.1})$$

$$\boxed{\left|\frac{F_y{}^B}{F_x{}^e}\right| = 2.74\times10^{-6}} \qquad (dimensionless) \tag{9.14}$$

In this case the Lorentz force would be a million times smaller than the electron wind force.

9.5 Unified Model for Atomic Flux during Electromigration

The atomic flux along the top and/or bottom interfaces of a conducting line, as illustrated in Figure 3.1, and in the presence of both a stress gradient and electron can be expressed as[28]:

$$J_a^i = \frac{D_i}{kT}\left[\nabla\sigma_n^i + \frac{F_e}{\Omega}\right] \tag{9.15}$$

For this assumption, i stands for either the top or the bottom surfaces of the line and σ_n^i is the normal traction for diffusion along the surfaces (stress). We also assume that the length of the conductor $L >> w$, where w is the conductor width. Diffusion along the x direction dominates and the diffusion along y direction is ignored. Therefore atomic flux J_a can be expressed as:

$$J_a^i = \frac{D_i}{kT}\left[\frac{\partial\sigma_n^i}{\partial x} + \frac{F_x^e}{\Omega}\right] \tag{9.16}$$

We have shown that B_z, the magnetic field at $y = \delta$ is given by $B_z(y = \delta) = \frac{\mu_0 Jt}{2\pi}\ln(\frac{W-\delta}{\delta})$. Equation 9.7. This is the magnetic field at $y = \delta$, due to current elsewhere in the conductor. Also the force F_y^B acting on a moving lattice atom under the influence of the magnetic field B_z is given by ${F_y}^B = -qvB_z$. Equation 9.6.

F_y^B acts in the negative y direction as illustrated in Figure 9.3.

Any given lattice atom at $y = \delta$ that is undergoing migration, has two perpendicular forces acting upon it at any given time and that resultant force F_{xy}^{eB} will be a vector sum of the forces F_x^e and F_y^B:

$$\left|F_{xy}^{eB}\right| = \sqrt{\left|F_x^e\right|^2 + \left|F_y^B\right|^2} \tag{9.17}$$

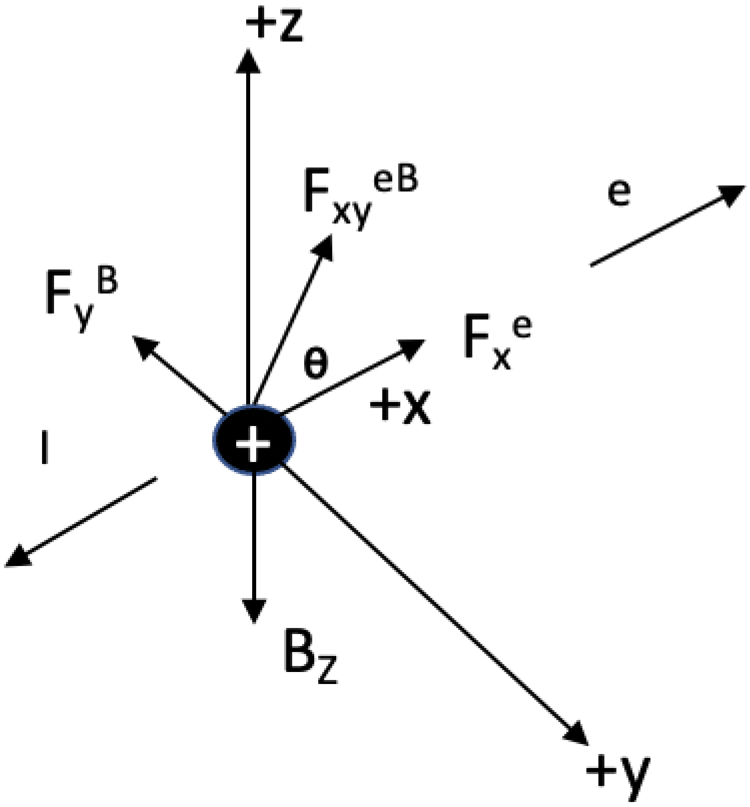

Figure 9.3: Vector sum of Magnetic force F_y^B and electron wind force F_x^e acting on a migrating lattice atom in the conductor.

$$\theta = \arctan \left| \frac{{F_y}^B}{{F_x}^e} \right| \tag{9.18}$$

Therefore, the atomic flux due to the Lorentz force, stress gradient and the electron wind force can be written as:

$$J_a^i = \frac{D_i}{kT} \left[\frac{\partial \sigma_n^i}{\partial x} + \frac{F_{xy}^{eB}}{\Omega} \right] \tag{9.19}$$

9.6 Significance of the Unified Model

The presented model predicts that there is a component of atomic flux which is not always in the direction of electron flow. The resultant magnitude and direction of atomic flux depends on the relative strengths of the electron wind and Lorentz forces acting on the migrating lattice ions. As estimated in the prior section, the Lorentz force F_y^B is about a million times smaller than the electron wind force F_x^e, under typical conditions, and therefore typically the ions undergo net migration in the general direction of electron flow. Efforts are underway to determine whether there are conditions where the Lorentz force is significant, such as when local current densities[39][40] are high enough to make it comparable to the electron wind force. Regions of high current density can be attributed to material transitions, geometry[41] along electromigration path and defects causing constriction to flow of carriers. Finally, the model assumes that the migrating atoms are ions and therefore considered to be non-neutral. Any migrating neutral atoms, if present, will not experience a Lorentz force. The model developed here ignores the possibility of neutral lattice atoms undergoing electromigration.

9.7 Magnetic Field Variation within the Conductor

The Lorentz force acting on the migrating ions depends on the magnetic field and therefore any variation of the magnetic field within the conductor will also determine any corresponding variations of the Lorentz force on the migrating ions.

Consider a cylindrical conductor of length L and with a cross sectional diameter of $2W$ as illustrated in 9.4.

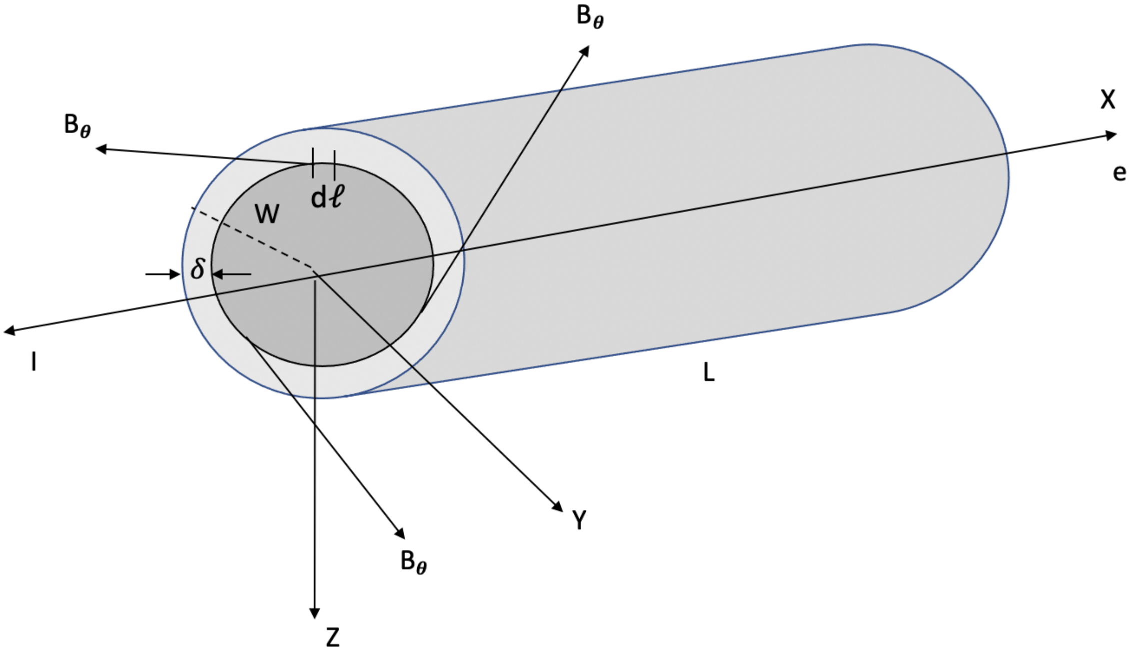

Figure 9.4: Magnetic field due to an element dl at a distance δ from the surface of a cylindrical conductor of diameter $2W$.

Using Ampere's Circuital Law:

$$\oint B_\theta \cdot dl = \mu_0 \cdot I_{enclosed} \tag{9.20}$$

Due to cylindrical symmetry, the magnetic field at every element dl, a distance δ from the surface, due to the electron flow is the same at every other point dl that will be at a distance δ from the surface. Therefore:

$$B_\theta \oint \cdot dl = \mu_0 \cdot I_{enclosed}$$

$$B_\theta \oint dl = B_\theta \cdot 2\pi \cdot (w - \delta)$$

$$I_{enclosed} = I \cdot \frac{(w-\delta)^2}{w^2}$$

$$B_\theta \cdot 2\pi \cdot (w-\delta) = \mu_0 I \cdot \frac{(w-\delta)^2}{w^2}$$

B_θ at a distance δ from the cylinder surface is then given by:

$$B_\theta = \frac{\mu_0 I}{2\pi} \cdot \frac{w-\delta}{w^2}$$

$$B_\theta = \frac{\mu_0 J}{2} \cdot (w-\delta) \tag{9.21}$$

As can be seen in Equation 9.21, the magnetic field is zero at the center of the cylinder ($\delta \to w$) and is a maximum at the cylindrical conductor's outer surface ($\delta \to 0$) Figure 9.5.

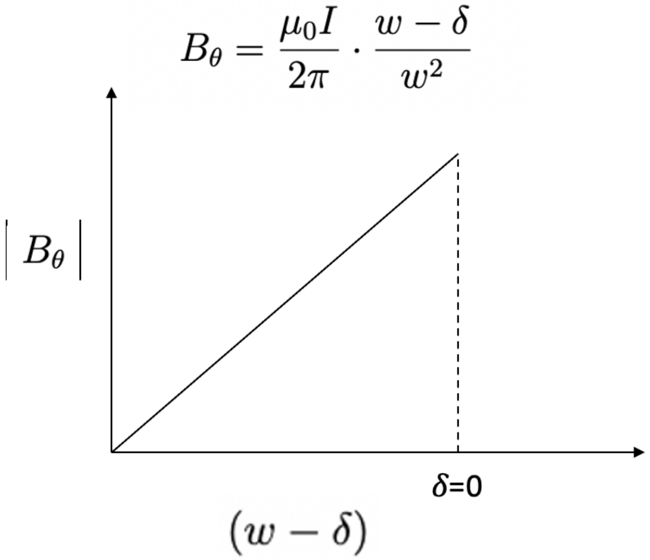

Figure 9.5: Magnetic field is zero at the center of the conductor ($\delta \to w$) and is a maximum at the conductor's outer surface ($\delta \to 0$).

The variation of the magnetic field from the center to the edges, Figure 9.5, has a similar trend for a rectangular conductor, Figure 9.2, where the magnetic field is zero at its center and maximum at the edges. This is easy to see from Equation 9.7.

9.8 Variation of the Lorentz Force and its Significance

The variation of the magnetic field from the center of the conductor to its edges means that the migrating ions in the center of the conductor will not experience any Lorentz force (Equation 9.6) while ions on the outer surface of the conductor will experience the maximum Lorentz force.

The Magnetic field and therefore Lorentz force on the migrating ions increases linearly from the center to the surface of the conductor as illustrated in Figure 9.6. In effect, there is a radial dilatation due to Lorentz forces on the drifting ions as the Lorentz force experienced by the atoms within the cross section is non-uniform. It is zero for lattice atoms on the central axis and maximum for those on the surfaces.

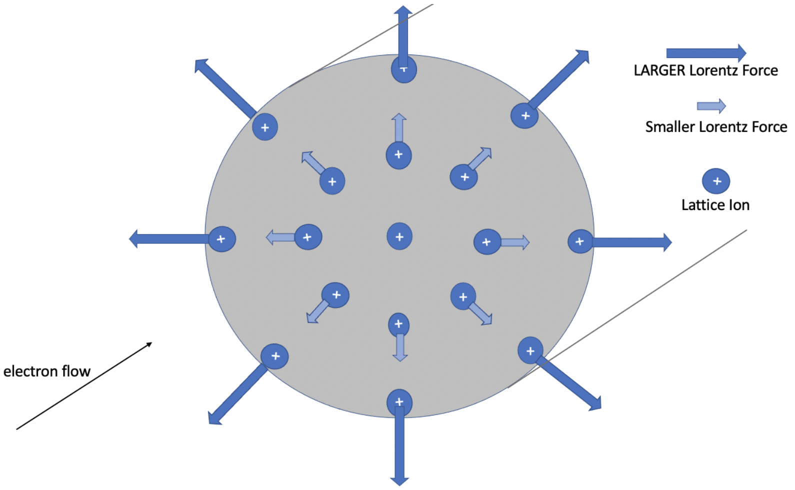

Figure 9.6: The variation of the magnetic field within a cylindrical conductor results in a corresponding variation in the Lorentz forces from center to the edge of the conductor.

In a conductor such as Copper, the transport is dominated by surface diffusion and the effect of Lorentz force on surface diffusion will be more prominent at regions within the conductor that are away from the center.

9.9 Impact of Lorentz Force on Void Morphological Evolution during Electromigration

Void morphological evolution under electric current has been widely studied by many groups[27, 42, 43, 44]. This typically involves analytically solving electric field and surface capillary forces around the void surface in order to theoretically predict the void's evolution. Wang and Yao[45] show analysis of electromigration-induced void morphological evolution using a theory of mass diffusion. They analyzed for three typical void shapes of circular, ellipse, and cardioid. It is the competition between the electron wind force due to the electric field and the surface capillary forces that determine the evolution path and shape of the void[45]. However, Wang and Yao's treatment is incomplete as the impact of the Lorentz forces on the void morphological evolution needs to be established. In this section we look at the void morphological evolution for a circular void that incorporates not only the impact of electric field induced electron wind forces and the surface capillary forces but also the Lorentz forces on the migrating lattice ions. A qualitative analysis is presented.

Figure 9.7 illustrates a void as described by Wang and Yao in their work. It is a two dimensional infinite conductor plane under the influence of an electric field E_∞. The void shape and position are evolving with time driven by diffusing ions along the surface of the void.

The diffusion process is governed by the component of the electromigration driving force along the void surface and the surface capillary force. While the electromigration driving force depends on the current density, the surface capillary force depends on the curvature of the void surface. Wang and Yao have shown that based on the Nernst-Einstein relation, the number of atoms per unit time passing along a unit length on a void surface is given by[46]:

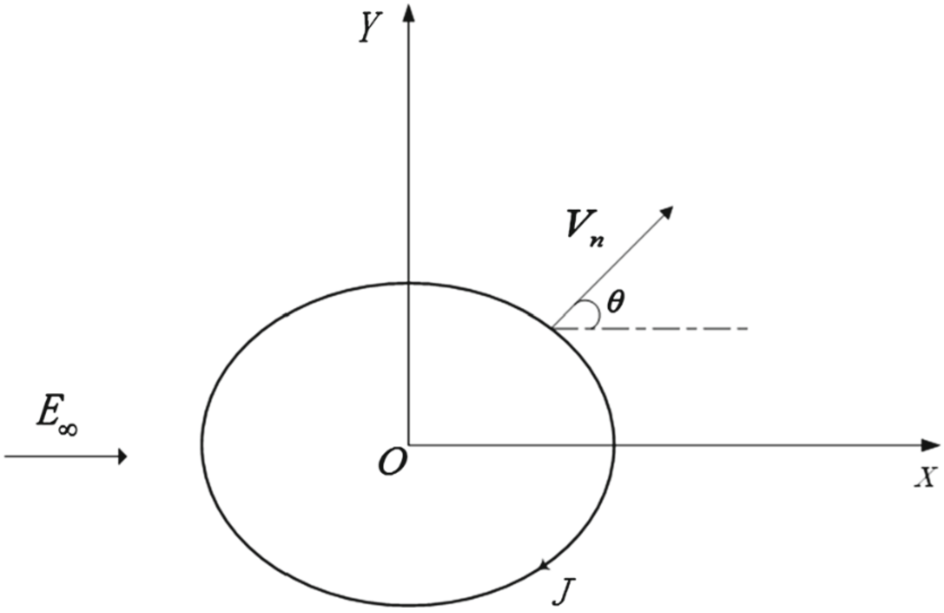

Figure 9.7: Wang and Yao's illustration of a void subjected to an electric field at infinity. V_n is the normal velocity of the void evolution on the surface.

$$J = \frac{D\delta_s}{\Omega KT}\left(- Z^* e E_t + \Omega\gamma\frac{d\kappa}{ds}\right) \tag{9.22}$$

where:

D is the surface diffusivity,

δ_s is the thickness of the surface layer,

Ω is the atomic volume,

K is the Boltzmann constant,

T is the temperature,

Z^* is the effective valence,

e is the electron charge magnitude,

E_t is the electric field tangent to the void surface

γ is the surface energy,

κ is the curvature of the surface at $\kappa = \frac{d\theta}{ds}$

Z^*eE_t is the electromigration driving force along the surface of the void

$\Omega\gamma\frac{d\kappa}{ds}$ is the capillary force on the void surface.

Wang and Yao have also shown that the normal velocity, V_n, at any point on the void surface is given by:

$$V_n = -\Omega\frac{dJ}{ds} \tag{9.23}$$

If F_x^e is the electromigration driving force in the direction of the electron flow then the tangential component of the electromigration driving force acting along the surface of the void is F_t^e and and given by Z^*eE_t, the electron wind force along the surface of the void.

When the void is a circle of radius R, the surface capillary force $\Omega\gamma\frac{d\kappa}{ds}$ disappears and therefore Wang and Yao's Equation 9.22 reduces to:

$$J = \frac{D\delta_s}{\Omega KT}\Big(- Z^*eE_t\Big) \tag{9.24}$$

Since $-Z^*eE_t$, the electromigration driving force acting along the surface of the void, is F_t^e, the equation can be re-written as follows:

$$J = \frac{D\delta_s}{\Omega KT}\Big(F_t^e\Big) \tag{9.25}$$

This representation is however incomplete as it does not include the effect of Lorentz forces acting on the migrating ions along the surface of the void. We have previously derived in Equation 9.17 that for any given lattice ion within the bulk of the conductor undergoing migration, there are two perpendicular forces acting upon it at any given time and that the resultant force F_{xy}^{eB} will be a vector sum of those two forces acting in the X-Y plane. For the ions migrating along the surface of the void, these component forces are F_t^e, the electromigration driving force acting tangentially and F_p^B, the Lorentz force, acting perpendicular to the void surface and also perpendicular to the tangential electromigration driving force of F_t^e. The magnitude of this resultant force is given by:

$$\left|F_{xy}^{eB}\right| = \sqrt{\left|F_t^e\right|^2 + \left|F_p^B\right|^2}$$

The angle θ, as illustrated in Figure 9.8, is given by:

$$\theta = \arctan\left|\frac{F_p^B}{F_t^e}\right|$$

A modified and a more accurate representation is needed for the flux of the migrating ions along the surface of the void, J, and for the normal velocity on the void surface V_n. Further work is needed for this analysis.

The electromigration driving force on the atoms along the surface of the void, F_t^e, always acts in a tangential direction. The Lorentz force F_p^B is acting in the radial direction and perpendicular to the electromigration driving force F_t^e but not always pointed towards the center of the void. Vacancies would therefore be created at the lower void surface and absorbed at the upper void surface. This results in the void to drift upward. As there is no electromigration drift on the side surfaces of the void, i.e. at points "A" and "B" in the Figure 9.8, the Lorentz and the electron wind forces are zero at these points. However, it is to be noted that the normal velocities on the void, represented by V_n are non-zero and

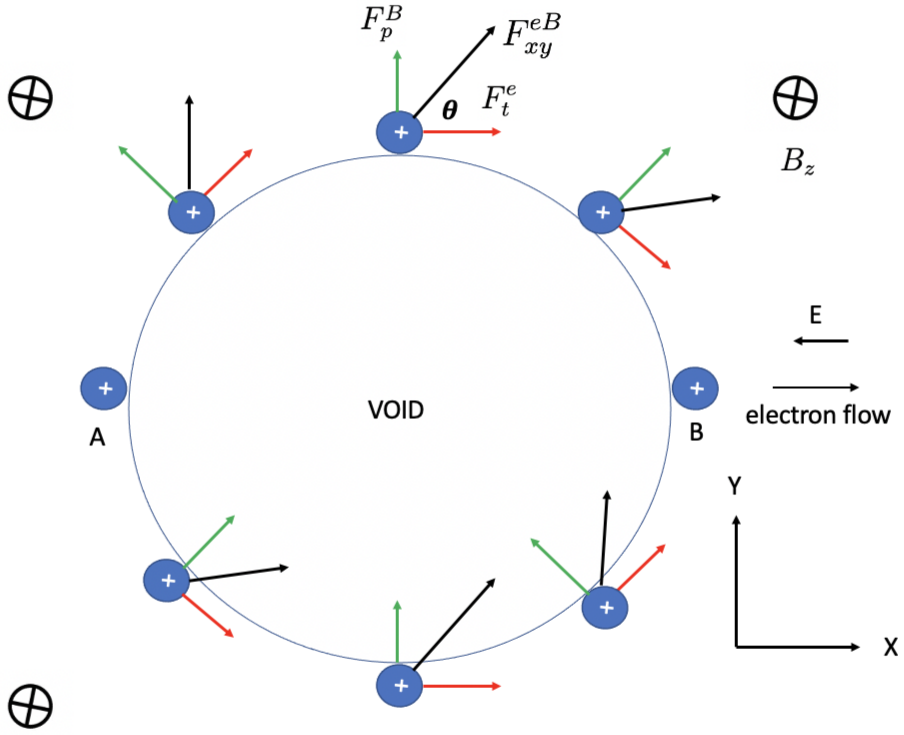

Figure 9.8: Electron wind and Lorentz forces acting on the migrating ions along the surface of a void in a conducting metal matrix. The magnetic field B_z is directed into the plane of the paper. No forces act on ions at points A and B. Void may move slightly downward as it is swept along to the left.

largest at points A and B because of mass accumulation or depletion at those points driven by diffusion rather than any ionic currents that may be present at those same points.

The significance of this qualitative analysis is determined by the strength of the Lorentz force relative to the electron wind force. We have shown that under typical electromigration conditions, the Lorentz force is a million times smaller than the electron wind force. Conditions that make the Lorentz force significant will result in void morphology evolution that may not move the void straight to the left, as suggested by Wang and Yao. The void may move slightly downward as it is swept along to the left. Such conditions were mentioned in Section 9.6 and some experiments to study the impact of Lorentz forces on void evolution are presented in Chapter 11.

Additional work is needed in the current analysis including further derivation of modified expressions for Flux J and normal velocity V_n for a more complete analysis using the component forces. This will be looked at as future work and ongoing research.

9.10 Other Considerations and Future Work

Until now we have discussed the impact of Lorentz force on lattice ions. As described elsewhere in detail, the moving electrons create a magnetic field that results in the Lorentz force acting on the migrating lattice ions. We now consider two other phenomena which can have additional impact and significance. These are mentioned briefly and qualitatively in the following sub-sections however details and quantitative treatment is beyond the scope of this dissertation and will be considered for future and ongoing research work in this field.

9.10.1 Elastic squeezing of the lattice due to Lorentz force on electrons

The electron flow that creates a magnetic field will also result in Lorentz forces on the moving electrons. Such a force on the electrons themselves has been reported to cause a ”Pinch Effect” leading to plastic deformation of metals[47]. It is possible that such ”Pinching” can result in an ”Elastic Squeezing” of the lattice ion. Unlike the Lorentz force on migrating ions that has been shown to act in the negative Y direction, the force due to pinching electrons would in effect squeeze or compress the lattice and for a cylindrical conductor such a pressure on the lattice would be directed radially towards the central axis of the conductor. Some preliminary analysis shows that the effect of electronic squeezing on the lattice may be insignificant, however, further research in this area is ongoing.

9.10.2 A new concept of ”Dielectric Drag”

It remains to be seen if dielectric behavior could contribute to atomic flux during electromigration. Hubbard[48] suggested that the Coulomb interaction of the electrons in solids can be understood by treating the solid as a homogeneous dielectric. The dielectric behavior can be interpreted on the atomic scale as immobility of electrons because they are held too tightly by the ions (leading to charge separation). Most materials, including conductors, are known to exhibit some degree of dielectric behavior. If electrons are flowing, but at the same time the ions are trying to prevent them from moving due to Coulomb forces, then perhaps the electrons have a tendency to drag the ions along with them. This is not the Lorentz force and is also in a direction different to the Lorentz force on the lattice ions, but perhaps it contributes to the atomic flux. We like to call this phenomenon as ”Dielectric drag”. Further research in this area is ongoing.

CHAPTER 10

CURRENT CROWDING AND SIMULATION

10.1 Literature Review on Current Crowding and Effect of Geometry

Current crowding[49] occurs whenever a current changes direction, for example, when passing through sharp corners or a via. It has been proposed[39] that in current crowding, the current-density gradient can exert a driving force strong enough to cause excess vacancies (point defects) to migrate from high to low current-density regions. This leads to void formation.

Current crowding affects electromigration adversely. It has been postulated by Tu and Yeh et al[39] that point defects such as vacancies and solute atoms have a lower probability of occurring in high current-density regions than in low current-density regions. The potential gradient in current crowding provides a driving force to displace these defects from high to low current-density regions. As a consequence, the voids tend to form in low current-density regions rather than in high current-density regions, which is contrary to intuition.

The concept of a driving force for vacancy diffusion due to a gradient in current density accounts for observations that voids often form in regions where no current is flowing. In this model[39], a chemical potential, P, is defined for a vacancy in a conductor carrying a current density, j , as:

$$P = q_v|j|A\Delta\rho_v \tag{10.1}$$

where q_v is the charge, A is the scattering cross section, and $\Delta\rho_v$ is the specific resistivity of the vacancy, respectively. It is argued that vacancies have a charge equivalent to the electromigration “effective charge,” z^*, and that they would move down a chemical potential gradient defined by the current crowding. The site where the current is the highest would have the greatest potential and the lowest current density, the least potential. Chemical potential gradients as high as 10 eV/cm were calculated[39].

10.2 Line Geometry and Electromigration Stress Simulations using MATLAB

Electromigration driven flux of lattice ions results in the evolution of mechanical stresses in the interconnects. Korhonen and Borgesen et al[50],[51] have derived solutions for the differential equation governing the evolution of back stresses during electromigration.
As described in earlier chapters, we derived a one-dimensional model for line stress during electromigration and implemented it as a numerical solution in chapters 3 and 4, respectively. We further used the MathCAD simulator tool to study geometry, temperature and current density effects on line stress and compared it with actual experimental data from other groups, as described in chapter 7. In the following sections we describe the line stress evolution adopted and modeled by other groups and attempt to simulate their one dimensional models for calculating evolved line stress using MATLAB. This is expected to provide useful insights on how abrupt changes in geometry may result in line stress variations as a function of stress time and position along the line geometry and therefore due to local current crowding.

10.2.1 Line Stress Equation of Korhonen

In the following section we present line stress evolution simulations for two different line geometries using the stress evolution equations for a one-dimensional metal line by Korhonen and Borgesen et al[51].

The widely used Korhonen's equation[50],[52] is given as follows:

$$\frac{\partial \sigma}{\partial t} = \frac{\partial}{\partial x}\left[k\left(\frac{\partial \sigma}{\partial x} + \frac{eZ\rho j}{\Omega}\right)\right] \tag{10.2}$$

Where:

$\kappa = DB\Omega/k_BT$

$D = D_0 \exp(-E_a/k_BT)$ is the atomic diffusivity,

B is the bulk modulus,

Ω is the atomic volume,

E_a is the activation energy,

k_B is Boltzmann's constant, and

eZ is the effective charges on the migrating lattice ions.

The temperature and current density are uniformly distributed along the length of the conductor.

10.2.2 Korhonen's Line Stress Equation as a Cosine Series

Huang et al[52] have shown that for a finite conductor of length l with blocked boundaries, Korhonen's equation has a solution for an initial-boundary value problem that can be shown to be an infinite Cosine series:

$$\sigma = \sigma_T + \frac{ez\rho jl}{\Omega}\left(\frac{1}{2} - \frac{x}{l} - 4\sum_{n=0}^{\infty}\frac{\cos(\frac{(2n+1)\pi x}{l}}{(2n+1)^2\pi^2}\, e^{-\kappa\frac{(2n+1)^2\pi^2}{t^2}}\right) \tag{10.3}$$

where, l is the length of the conductor, j is the current density, σ_T is the evolved mechanical stress at temperature T.

10.2.3 Test Structure Geometry for MATLAB Simulation

A simple test geometry was realized in order to study the effect of an abrupt change in current density on the stress evolution along the conducting line with the help of computer simulations using MATLAB.

The line stress buildup simulations were run on a conductor of uniform cross-section for a control data-set and the simulations repeated on another conductor geometry of equal length and material properties, except that the cross-sectional area in the middle of the conductor was abruptly reduced for about 60μ compared to elsewhere in the conductor with a total length of $L = 100\mu$. The line basic assumptions and geometry are described in Table 10.1 and as illustrated in Figure 10.1.

Table 10.1: Material properties and line geometry assumptions for Matlab simulations

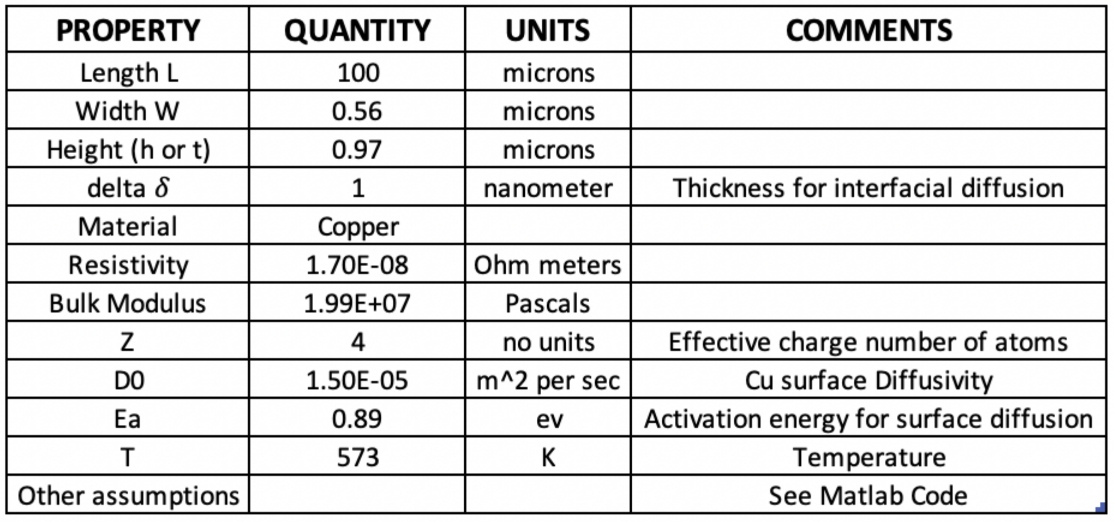

PROPERTY	QUANTITY	UNITS	COMMENTS
Length L	100	microns	
Width W	0.56	microns	
Height (h or t)	0.97	microns	
delta δ	1	nanometer	Thickness for interfacial diffusion
Material	Copper		
Resistivity	1.70E-08	Ohm meters	
Bulk Modulus	1.99E+07	Pascals	
Z	4	no units	Effective charge number of atoms
D0	1.50E-05	m^2 per sec	Cu surface Diffusivity
Ea	0.89	ev	Activation energy for surface diffusion
T	573	K	Temperature
Other assumptions			See Matlab Code

10.2.4 MATLAB Code for Simulation

The MATLAB simulation presented here is limited to calculation of line stress evolution without consideration given to magnetic fields and Lorentz forces. Lorentz forces from such fields are not part of the simulation. The simulation is to show the effect of abrupt change in current density only on line stress evolution. We have modeled the effect of

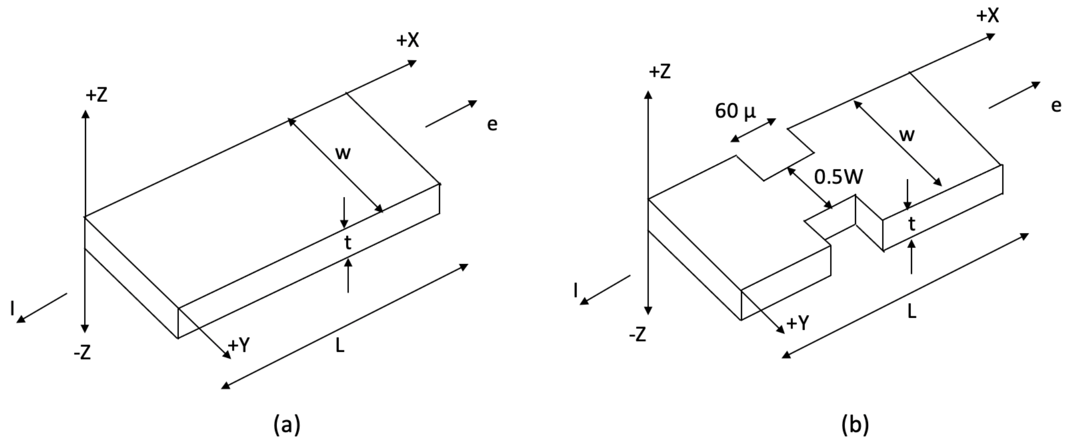

Figure 10.1: (a) Geometry of control unit with uniform cross-sectional area, (b) Geometry of simulation unit. Both (a) and (b) have similar thickness t, length L and average current density $j = I/(w \times t)$ except along a length of 60μ, as illustrated, where the width w is halved in simulation unit, resulting in twice the local current density.

magnetic fields on atomic flux in this dissertation. The simulation of magnetic fields and resulting Lorentz forces for line stress evolution is out of scope for this dissertation but efforts will be underway as future and ongoing research.

Korhonen's line stress equation represented as a Cosine series (Equation 10.3) is a one dimensional equation for line stress evolution. We have coded this in MATLAB to conduct simulation studies for one specific geometry. This section lists the MATLAB code for the control unit in its entirety.

```
% BEGIN MATLAB CODE
%
%
%
% Author:   Rao Morusupalli
% Date:     June, 2021
% Purpose:  Conducting Line Stess build-up calculations
% Inputs:   Current Density, Temperature, line dimensions, Material properties etc
% Outputs:   Stress along lenghth of conducting line

clc
clear
clf (figure(1))
```

```

%%%%%%%%%%%%%%%%%%%%%%%%%%%%%%%%%%%%%%%%%%%%%%%%%%%%%%%%%%

% Line Geometry Assumptions
L = 100e-6;              % meters (100 microns), Line length = L
a = 0.35e-6;            % meters, 2a = 0.56 microns, line width = 2a
delta = 1e-9;           % meters, Thickness of interface
h = 0.97e-6;            % meters, h = 0.97 microns, line thickness = h

% Basic Constants
q = 1.6e-19;            %(C) Electronic Charge
kB = 1.38e-23;          %(m^2.kg.s^2.K^-1) Boltzmann Constant

% Material properties of Copper - original in Dissertation using MathCAD
resistivity_Cu = 1.7e-8;% ohm-meters, Resistivity
%M = 7e10;               %(Pa)% % pascals, Plane Strain Modulus
% Other Material properties of Copper
B = 1.99e7;               %(Pa)% % Pascals, Bulk Moduloius Modulus
% NOTE M = Plane Strain Elastic Modulous is B*[(2*pi*a)/delta]
% NOTE B = M*(delta)/(2*pi*a)
% M assumed for MATHCAD simulations was 7e10 therefore B assumed here is
% 1.99e7
Z = 4;                  % effective charge number of atoms
D0 = 15e-6;             % Cu Diffusivity (Surface=15e-6, GB=5e-6, m^2
   per sec
Ea = 0.89*q;            % 86.65 Kilo Joules per mole = 86.65/96.487 =
   0.89eV, 1 ev = 96.487 kJ/mol
Omega = 1.18e-29  ;     % cubic meters, Atomic volume

% Note on D0 and Ea conversions
% Activation Energies in ev and KJ per mole
% Cu GB Diffusion
    %(D0 = 5e-6 m^2 per sec), Ea = 104 KJ per mole = 1.078eV
% Cu Surface Diffusion
    %(D0 = 15e-6 m^2 per sec), Ea = 86.65 KJ per mole = 0.89ev



rstress=0;              %(Pa) residual stress

%%%%%%%%%%%%%%%%%%%%%%%%%%%%%%%%%%%%%%%%%%%%%%%%%%%%%%%%%%%
% Simulation parameters:
% T = Temperature in degrees K%
% curden: Current density
% jlocmax: Maximum line lenght
% jlocstep: step distance along line
                           %
% loc: Coordinate along the wire
%%%%%%%%%%%%%%%%%%%%%%%%%%%%%%%%%%%%%%%%%%%%%%%%%%%%%%%%%%%
T = 573; %(K)
curden = 10e9; %(A.m^-2)

jlocmax = 100e-6; % cathode end
jlocstep = 0.02e-4;
```

```
jloc = 0:jlocstep:jlocmax;

deltaupon2pia = (delta/(2*a*pi));
Fe = q*Z*resistivity_Cu*curden; %Electron Wind Force in NEWTONS
G = (deltaupon2pia)*(Fe)/Omega; %Outside multipler in Cosine Series
%G = q*Z*resistivity_Cu*curden/Omega; %Outside multipler in Cosine
    Series
kappa = D0*exp(-Ea/kB/T)*B*Omega/kB/T; %Factor inside Cos series
    summation

%%%%%%%%%%%%%%%%%%%%%%%%%%%%%%%%%%%%%%%%%%%%%%%%%%%%%%%%%%
% calculate stress (EM stress + residual_stress) along the line length
%%%%%%%%%%%%%%%%%%%%%%%%%%%%%%%%%%%%%%%%%%%%%%%%%%%%%%%%%%
M = size(jloc,2);
stress = zeros(M,1);
N = 100;
eta = (1:2:2*N-1)'*pi/L;

%set various simulation run times, t, here (seconds)
t1 = 1*3600;
t2 = 25*3600;
t3 = 50*3600;
t4 = 100*3600; % 30 hours

for j = 1:M
    phi = (cos(eta*jloc(j)))./(eta.^2*L^2.*exp(eta.^2.*kappa*t1));
    stress1(j) = G*L*(0.5-jloc(j)/L-4*sum(phi))+rstress;

    phi = (cos(eta*jloc(j)))./(eta.^2*L^2.*exp(eta.^2.*kappa*t2));
    stress2(j) = G*L*(0.5-jloc(j)/L-4*sum(phi))+rstress;

    phi = (cos(eta*jloc(j)))./(eta.^2*L^2.*exp(eta.^2.*kappa*t3));
    stress3(j) = G*L*(0.5-jloc(j)/L-4*sum(phi))+rstress;

    phi = (cos(eta*jloc(j)))./(eta.^2*L^2.*exp(eta.^2.*kappa*t4));
    stress4(j) = G*L*(0.5-jloc(j)/L-4*sum(phi))+rstress;
end

figure(1)
hold on
plot(jloc,stress1,'-xr','linewidth',1.5)
plot(jloc,stress2,'-xb','linewidth',1.5)
plot(jloc,stress3,'-xg','linewidth',1.5)
plot(jloc,stress4,'-xm','linewidth',1.5)
xlabel('distance along line (m)','fontsize',16)
ylabel('stress(Pa)','fontsize',16)
set(gca,'fontsize',12)
title('Stress evolution under constant current load')
subtitle('Uniform Conductor')
ax = gca;
ax.TitleFontSizeMultiplier = 1.5;
ax.Color = 'white';
set(gca,'YLim',[-3e5, 3e5]);
set(gca,'XLim',[0, 100e-6]);
```

```
legend('t=1 hour','t=25 hours','t=50 hours', 't=100 hours')
grid on
grid minor
%
%
%
% END MATLAB CODE
```

10.2.5 Simulation Results and Discussion

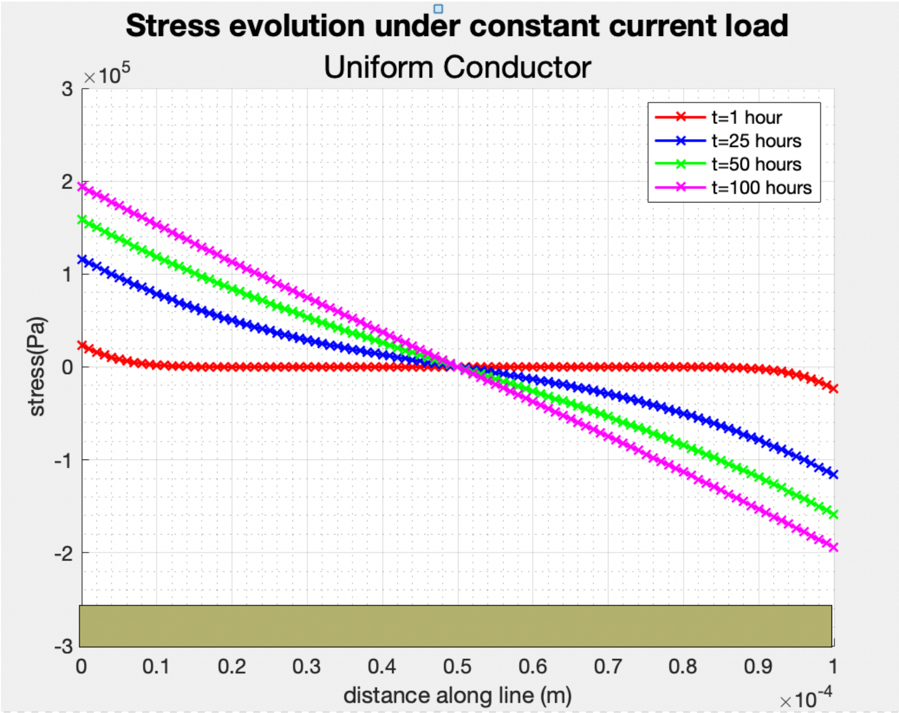

Figure 10.2: Stress evolution in a ”Uniform cross-section” conductor under constant current load. Simulation time ”t” shown in hours. Stress saturates at t=100 hours.

In prior simulation work using MathCAD and as described in previous sections, two limiting cases were studied. In the current simulation work using MATLAB, only one basic limiting case is presented. It was assumed that the interface can be treated like a free surface of Cu. Such an assumption is in line with real world diffusion paths observed during electromigration in Cu. Stress was calculated and plotted along regular intervals for a 100μ Cu line. The interface thickness was assumed to be 1 nm, probably an upper bound estimate. If surface diffusion is assumed for a Cu line simulated at 373^0K and with

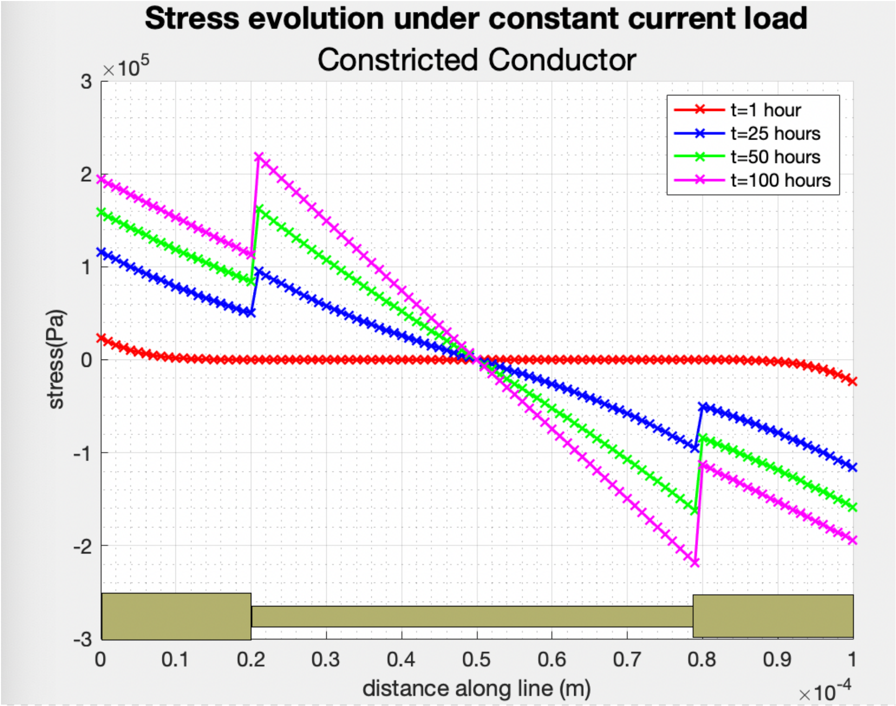

Figure 10.3: Stress evolution in a ”Constricted cross-section” conductor under constant current load. Simulation time ”t” shown in hours.

a current density of $10mA$ per square micron then the stress that develops under these conditions at a point on the line just before $L = 20\mu$ from the anode is about 100 KPa, at time $t = 100 hours$. This is the point along the line where the cross-section is abruptly reduced by a factor of 0.5. The stress immediately after $L = 20\mu$ is about 200KPa. This increase of stress in the constricted geometry is seen all along the constriction length when compared to the control geometry as illustrated in the simulation plots shown in Figure 10.2 and Figure 10.3. These stresses are probably too small to initiate voiding, but the conditions that have been assumed do not lead to failure.

The abrupt increase in evolved stress along the line is also higher for longer duration of the stress times. Additionally, the stress seems to increase in the constricted part of the conducting line even when the evolved stress was otherwise saturated. These are highlighted in the simulation plots shown in Figure 10.4.

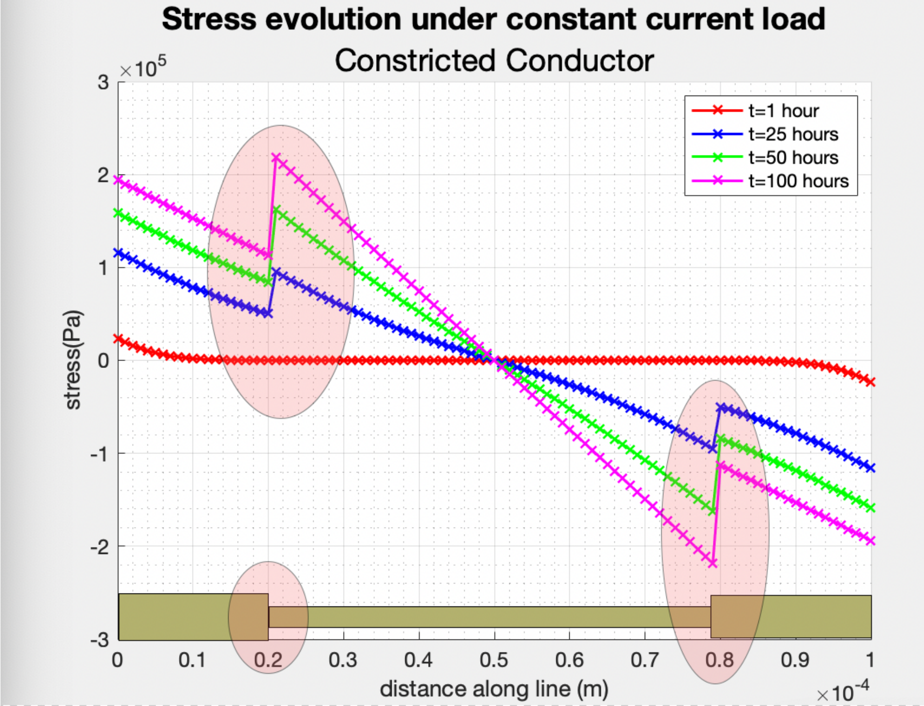

Figure 10.4: Stress evolution in a ”Constricted cross-section” conductor follows the abrupt change in cross-sectional area. More pronounced for longer stress durations.

In conclusion, the simulation results presented here show that abrupt changes in geometry not only cause the expected changes in current density but also abrupt changes in stress evolution that results due to electromigration. Further research is needed to combine the presented effects of geometry and stress with magnetic fields and Lorentz forces and this work is noted for future and ongoing research work.

CHAPTER 11

SUGGESTED EXPERIMENTS

In this chapter some experimental suggestions are presented to study the effect of Lorentz force on defects and voids during the process of electromigration. The approach and propositions are high level recommendations. The actual conduction of the experiments or the sample fabrication is out of scope of this dissertation. As the model of atomic flux developed in this work is new and there are no prior data points available in literature for study of the direct impact of Lorentz forces on atomic flux during electromigration, the actual experimental methods that may be designed and implemented are expected to have much flexibility and variations.

11.1 Experiment to Study the Effect of Lorentz Force on Void Growth

The variation of the magnetic field and Lorentz force and its effect and significance have been discussed qualitatively in the previous Chapter. We now present the specifics of some suggested experiments to study the effect of Lorentz force on void growth.

11.1.1 In-situ Observations of voids in general

Some prior work in the observation of void growth and motion not related to Lorentz forces is presented here as motivation for a similar study and visualization of the effect of Lorentz forces on voids for electromigrating metal lines.

Meyer, Hermann, Langer and Zschec[53] have designed and demonstrated a study of void growth during electromigration using in-situ experimentation on fully passivated cross-sections of copper interconnects. This setup enables demonstration of the effect of flux divergence and grain boundaries by presenting an SEM (Scanning Electron Microscopy) / FIB (Focussed Ion Beam) visualization of actual growth and motion of the voids. Choi and Thompson et al[54] have conducted similar experiments using in-situ SEM and performed observations on copper interconnects to study and demonstrate void formation and growth including studies to correlate void formation to line widths.

11.1.2 In-situ Observations for effect of Lorentz force

In order to study and visualize the effect of magnetic field induced Lorentz force, an in-situ setup similar to as described in Section 11.1.1 can be used with special emphasis on location of the voids. This is because the novel model presented in section 9.5 predicts that the effect of Lorentz force on defects and voids is minimal at the center and the central axis of the conductor and becomes maximum at its outer surfaces.

11.1.3 Suggested methods for Fabrication of voids for experimental samples

Since the formation of defects and voids in an interconnect depends on materials and impurities, fabrication technology, line widths and test structure geometry, it can be challenging to fabricate voids of predetermined size and location within an experimental interconnect sample. As described in the previous section, for a controlled experiment, time zero voids at both the center and the outer surfaces of the interconnect need be fabricated to study the variation of the effect of Lorentz force within an interconnect described in previous sections.

If placement of defects and voids with a predetermined size and location within a sample is not practicable, one can study the variation of void growth and their migration by comparing a significant number of random and intrinsic voids that are naturally formed due to any fabrication process. It should be possible to conduct in-situ observations on these fabricated defects and voids by grouping their behavior and variation from center to the edge of the conducting line.

Significant research results by other groups on the reduction of voiding in metal lines with the aim of reducing stress voiding and improving electromigration lifetime is available in the literature[55]. In copper interconnect lines the interface between the cap layer and the metal is a region of fast diffusion path. A sub-optimized cap layer can therefore induce defects at the surface of a metal line. Similarly, looking at techniques that reduce the defects and voids within the bulk of an interconnect line can provide practical insights to point defects and voids within the bulk region for the sake of creating experimental samples with known defect size, density and location within the conductor. Daniel et al [56] have demonstrated the effect of copper seed aging on void formation in single crystal copper. Wetting of copper is compromised during copper electroplating due to oxide formation caused by copper seed aging. Controlling the aging of seed copper can therefore control void size, density and location.

Actual fabrication of samples is beyond the scope of this dissertation.

11.2 Experiment to Study the Effect of Current Crowding on Lorentz Force

As stated in section 10.1, it has been proposed[39] that during current crowding, the current-density gradient can exert a driving force strong enough to cause excess vacancies (point defects) to migrate from high to low current-density regions. This leads to void formation.

Park et al[57] have simulated and tested structures with different levels of current crowding and tested its impact on electromigration lifetime.

Localized magnetic field strength may be much higher due to higher local current density. The Lorentz for ${F_y}^B$ depends on the magnetic field (equations 9.6 and 9.9) and therefore the current density j for a fixed line thickness t. Although the effect of current crowding on void formation and its dynamics has been studied[57], the effect of current crowding on Lorentz force experienced by migrating lattice ions is less investigated.

11.2.1 Suggested test structure geometries for effect of current crowding on Lorentz Force

Here we suggest experiments and test structures to compare the effect of Lorentz force on void growth with current crowding as a factor. The in-situ void growth observations suggested in the previous sections can be performed on specific test structures described in this section that increase local current crowding while maintaining a uniform average current density.

We expect either enhanced or reduced void growth and migration in areas of excess local current crowding. The effect of Lorentz force on void growth and migration is expected to be most pronounced in the outer regions of the conductor and minimal in the central axis regions. Additionally, similar to line-via interfaces in real life interconnects, right angle bends in the suggested test structures can help understand the effect of magnetic fields at such transition locations..

With this in mind, the suggested test samples have current crowding that is targeted in the outer regions of the conductor (figure 11.1), while maintaining a near uniform conductor current density and overall length that is similar between the test and control structures.

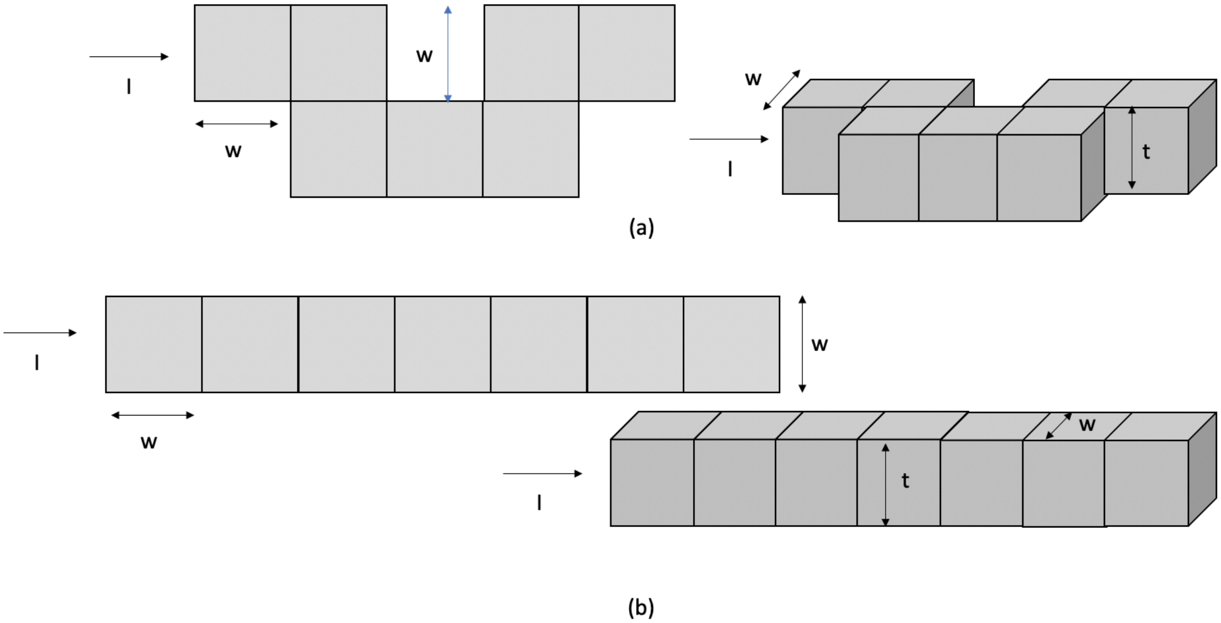

Figure 11.1: (a) Top and side view of current crowding test structure, (b) Top and side view of control structure. Both (a) and (b) have same width w, thickness t, length $7w$ and average current density $j = I/(w \times t)$. Note: The structures are proposed to be continuous metal lines. The square pieces in the illustration are for reference only.

11.3 Experiment to Verify the Impact of Lorentz Force using an Externally Applied Magnetic Field

In chapter 9.4 it was shown that the Lorentz force is about a million times smaller than the Electron wind force acting on the migrating lattice ions. For the simple geometry of an interconnect as illustrated in Fig 9.2 and with the same assumptions that were made to estimate the Lorentz force, it can be shown that at a distance $\delta = 1nm$ from the conductor's edge, the magnetic field due to electron flow elsewhere in the conductor is approximately $1.38 \times 10^{-3}\, Tesla$.

One can produce magnetic fields as high as 20 or 30 $Tesla$ in a laboratory facility. If a magnetic field of 13.8 $Tesla$, which is four orders of magnitude larger than the intrinsically generated magnetic field of $1.38 \times 10^{-3}\, Tesla$, can be applied, then the Lorentz force as calculated in section 9.4 will be as large as one percent of the electromigration driving force. This might have an observable effect to study the impact of the externally produced

Lorentz force. It would serve as a proof of concept that the Lorentz force does have an impact on elecgtromigration flux and void formations.

If one could subject an aluminum or copper conductor to such a strength of an externally applied magnetic field, then there might be a force large enough to sweep ions from one side of the line to the other, creating tensile stresses on one interface and compressive stresses on the other. The tensile stresses might lead to voids at the edge of the line subjected to tension.

Conducting such an experiment, with a very large and externally applied magnetic field, will ratify the theory of the impact of Lorentz force of any magnitude including the Lorentz force generated by intrinsic magnetic fields due to flow of electrons during electromigration. Additionally, such a high magnetic field experiment could help to prove that the mass migration caused by electromigration involves the flow of ions and not neutral atoms, which would not be subjected to Lorentz forces.

CHAPTER 12

CONCLUSIONS

A one dimensional model was developed for simulation of electromigration-induced stress in VLSI interconnect structures using a model of electromigration induced stress. The effects of line geometries and overhangs, material properties and electromigration stress conditions have been included in the simulation using the MATCHCAD tool. The tool has been used to simulate electromigration-induced stress in pure Cu interconnects, but it can be applied for any pure interconnect material. The tool was also used for comparing available experimental data with generated simulated data for stress evolution in a line.

A new model for atomic flux during electromigration that includes the effect of magnetic fields on migrating ions, due to electron flow elsewhere in a conductor, has been derived. It includes Lorentz force acting on the migrating ions. This force was not previously included as a factor in widely used models of atomic flux during electromigration.

Under typical conditions the Lorentz force is a million times smaller than the electron wind force. It remains to be determined if conditions exist where the Lorentz force can be a significant factor impacting electromigration damage and lifetime. The impact of Lorentz force on void morphological evolution during electromigration was qualitatively analyzed. Initial analysis shows that significant amount of Lorentz force can result in void evolution that is not necessarily towards the cathode. Further research is needed in this field.

Some simulation work is presented using tools such as MATLAB in order to investigate how current density variations along the cross-section and geometry of a conductor result in stress variations that may result in enhancing the significance of the investigated Lorentz forces for atomic flux. Further research is needed in this area as well. Further work is also necessary to understand newly proposed phenomena such as ”Lattice squeezing” due to magnetic fields on flowing electrons and a newly proposed concept of ”Dielectric drag”. Some preliminary analysis shows that the effect of electronic squeezing on the lattice may be insignificant. These will be looked at as future work and ongoing research.

Experimental methods and sample fabrication techniques for void formation and their location control are suggested to study the effect of Lorentz force on defects and voids during the process of electromigration. The actual fabrication and testing is out of scope for this dissertation but will be looked as future work for ongoing research.

Finally, electromigration continues to be a major reliability concern in the semiconductor chip industry. With current silicon technology nodes reaching under $5nm$ critical dimensions, the issues associated with reliability of today’s interconnects in microelectronic devices is even more critical to product lifetime. It is important to understand the root cause of intrinsic and extrinsic defects and voids in a metal line. Many are unanswered today. A deeper understanding of void formation and dynamics and the role played by intrinsically generated Lorentz forces during electromigration can throw new light in understanding the issues and optimizing interconnect design for improved product lifetime and reliability.

Bibliography

[1] J.R. Black. Electromigration—a brief survey and some recent results. *IEEE Transactions on Electron Devices*, 16(4):338–347, 1969.

[2] Rolf Landauer and James W. F. Woo. Driving force in electromigration. *Phys. Rev. B*, 10:1266–1271, Aug 1974.

[3] Mathcad PTC. 14.0. *User's Guide (pdf)*, 2007.

[4] AV Vairagar, SG Mhaisalkar, and Ahila Krishnamoorthy. Electromigration behavior of dual-damascene cu interconnects—-structure, width, and length dependences. *Microelectronics Reliability*, 44(5):747–754, 2004.

[5] The Mathworks, Inc., Natick, Massachusetts. *MATLAB version 9.3.0.713579 (R2017b)*, 2017.

[6] K. N. Tu, C. C. Yeh, C. Y. Liu, and Chih Chen. Effect of current crowding on vacancy diffusion and void formation in electromigration. *Applied Physics Letters*, 76(8):988–990, 2000.

[7] Wm G Hoover. Molecular dynamics. In *Molecular Dynamics*, volume 258, 1986.

[8] Steve Plimpton. Fast parallel algorithms for short-range molecular dynamics. *Journal of computational physics*, 117(1):1–19, 1995.

[9] James G Ryan, Robert M Geffken, Neil R Poulin, and Jurij R Paraszczak. The evolution of interconnection technology at ibm. *IBM Journal of Research and Development*, 39(4):371–381, 1995.

[10] JR Lloyd. Quick tests for electromigration: useful but not without danger. In *MRS Proceedings*, volume 265, page 177. Cambridge Univ Press, 1992.

[11] James R Black. Mass transport of aluminum by momentum exchange with conducting electrons. In *Reliability Physics Symposium, 1967. Sixth Annual*, pages 148–159. IEEE, 1967.

[12] IA Blech. Electromigration in thin aluminum films on titanium nitride. *Journal of Applied Physics*, 47(4):1203–1208, 1976.

[13] MJ Attardo and R Rosenberg. Electromigration damage in aluminum film conductors. *Journal of Applied Physics*, 41(6):2381–2386, 1970.

[14] P Shewmon. Diffusion in solids tms. *Warrendale, PA*, page 22, 1989.

[15] Inderjeet Kaur, Yuri Mishin, and Wolfgang Gust. Fundamentals of grain and interphase boundary diffusion. 1995.

[16] James R Black. Electromigration failure modes in aluminum metallization for semiconductor devices. *Proceedings of the IEEE*, 57(9):1587–1594, 1969.

[17] RJ Gleixner and WD Nix. A physically based model of electromigration and stress-induced void formation in microelectronic interconnects. *Journal of applied physics*, 86(4):1932–1944, 1999.

[18] Conyers Herring. Diffusional viscosity of a polycrystalline solid. *Journal of Applied Physics*, 21(5):437–445, 1950.

[19] HA Le, Larry Ting, NC Tso, and CU Kim. Analysis of the reservoir length and its effect on electromigration lifetime. *Journal of materials research*, 17(01):167–171, 2002.

[20] Hazara S Rathore, RG Filippi, RA Wachnik, Jose J Estabil, and Thomas Kwok. Electromigration and current-carrying implications for aluminum-based metallurgy with tungsten stud via interconnections. In *Microelectronic Processing'92*, pages 251–262. International Society for Optics and Photonics, 1993.

[21] C-K Hu, MB Small, and PS Ho. Electromigration in al (cu) two-level structures: Effect of cu and kinetics of damage formation. *Journal of applied physics*, 74(2):969–978, 1993.

[22] JC Blair. Concerning electromigration in thin films. *Proceedings of the IEEE*, 59(6):1023–1024, 1971.

[23] M Shatzkes and JR Lloyd. A model for conductor failure considering diffusion concurrently with electromigration resulting in a current exponent of 2. *Journal of Applied Physics*, 59(11):3890–3893, 1986.

[24] R Kirchheim and U Kaeber. Atomistic and computer modeling of metallization failure of integrated circuits by electromigration. *Journal of Applied Physics*, 70(1):172–181, 1991.

[25] JJ Clement and CV Thompson. Modeling electromigration-induced stress evolution in confined metal lines. *Journal of applied physics*, 78(2):900–904, 1995.

[26] JR Lloyd. Electromigration failure. *Journal of Applied Physics*, 69(11):7601–7604, 1991.

[27] William D Nix and Eduard Arzt. On void nucleation and growth in metal interconnect lines under electromigration conditions. *Metallurgical Transactions A*, 23(7):2007–2013, 1992.

[28] HB Huntington and AR Grone. Current-induced marker motion in gold wires. *Journal of Physics and Chemistry of Solids*, 20(1):76–87, 1961.

[29] Daniel B. Butrymowicz. Diffusion rate data and mass transport phenomenon for copper systems. *INCRA monograph series V*, 1977.

[30] Reese E Jones, Jeremy A Templeton, Gregory J Wagner, David Olmsted, and Nomand A Modine. Electron transport enhanced molecular dynamics for metals and semi-metals. *International Journal for Numerical Methods in Engineering*, 83(8-9):940–967, 2010.

[31] Di E Xu, Michael D Hook, and Michael Mayer. Molecular dynamics study of nanoscale ag surface electromigration and effect of pd coating layer. *dynamics (VMD)*, 32:33, 2014.

[32] Di E. Xu, Michael D. Hook, and Michael Mayer. Molecular dynamics study of nanoscale ag surface electromigration and effect of pd coating layer. In *14th IEEE International Conference on Nanotechnology*, pages 640–644, 2014.

[33] William Humphrey, Andrew Dalke, and Klaus Schulten. VMD – Visual Molecular Dynamics. *Journal of Molecular Graphics*, 14:33–38, 1996.

[34] John Stone, Justin Gullingsrud, Paul Grayson, and Klaus Schulten. A system for interactive molecular dynamics simulation. In John F. Hughes and Carlo H. Séquin, editors, *2001 ACM Symposium on Interactive 3D Graphics*, pages 191–194, New York, 2001. ACM SIGGRAPH.

[35] J Rud Nielsen. Hans christian oersted—scientist, humanist and teacher. *American Journal of Physics*, 7(1):10–22, 1939.

[36] FW Schott. On the biot-savart law. *IEEE Transactions on Education*, 25(1):39–39, 1982.

[37] David L Littlefield. Thermomechanical and magnetohydrodynamic stability of elongating plastic jets. *Physics of Fluids*, 6(8):2722–2729, 1994.

[38] DL LITTLEFIELD. Magnetomechanical instabilities in elastic-plastic cylinders, part i: Elastic response. *Journal of applied mechanics*, 63(3):734–741, 1996.

[39] KN Tu, CC Yeh, CY Liu, and Chih Chen. Effect of current crowding on vacancy diffusion and void formation in electromigration. *Applied Physics Letters*, 76(8):988–990, 2000.

[40] H. Wang, C. Bruynseraede, and K. Maex. Impact of current crowding on electromigration-induced mass transport. *Applied Physics Letters*, 84(4):517–519, 2004.

[41] Yongkun Liu, C. L. Cox, and R. J. Diefendorf. Finite element analysis of the effects of geometry and microstructure on electromigration in confined metal lines. *Journal of Applied Physics*, 83(7):3600–3608, 1998.

[42] GM Pharr and WD Nix. A numerical study of cavity growth controlled by surface diffusion. *Acta Metallurgica*, 27(10):1615–1631, 1979.

[43] SJ Subramanian, P Sofronis, and P Ponte Castaneda. Void growth in power-law creeping solids: Effect of surface diffusion and surface energy. intern. j. of solids and structures, vol. 42, is. 24-25, 6202-6225, 2005.

[44] Paul S Ho. Motion of inclusion induced by a direct current and a temperature gradient. *Journal of Applied Physics*, 41(1):64–68, 1970.

[45] Yuexing Wang and Yao Yao. A theoretical analysis of the electromigration-induced void morphological evolution under high current density. *Acta Mechanica Sinica*, 33(5):868–878, 2017.

[46] Z Suo, W Wang, and M Yang. Electromigration instability: Transgranular slits in interconnects. *Applied Physics Letters*, 64(15):1944–1946, 1994.

[47] O. A. Troitskii. Pinch-effect-induced plastic deformation of metals. *Fiziko Khimicheskaia Mekhanika Materialov*, 13:46–50, December 1977.

[48] J Hubbard. The dielectric theory of electronic interactions in solids. *Proceedings of the Physical Society. Section A*, 68(11):976–986, nov 1955.

[49] Everett CC Yeh, WJ Choi, KN Tu, Peter Elenius, and Haluk Balkan. Current-crowding-induced electromigration failure in flip chip solder joints. *Applied physics letters*, 80(4):580–582, 2002.

[50] MA Korhonen, P Bo/rgesen, King-Ning Tu, and Che-Yu Li. Stress evolution due to electromigration in confined metal lines. *Journal of Applied Physics*, 73(8):3790–3799, 1993.

[51] 5_M A Korhonen, P Bo/rgesen, DD Brown, and Che-Yu Li. Microstructure based statistical model of electromigration damage in confined line metallizations in the presence of thermally induced stresses. *Journal of applied physics*, 74(8):4995–5004, 1993.

[52] Xin Huang, Valeriy Sukharev, Taeyoung Kim, Haibao Chen, and Sheldon X-D Tan. Electromigration recovery modeling and analysis under time-dependent current and temperature stressing. In *2016 21st Asia and South Pacific Design Automation Conference (ASP-DAC)*, pages 244–249. IEEE, 2016.

[53] M.A Meyer, M Herrmann, E Langer, and E Zschech. In situ sem observation of electromigration phenomena in fully embedded copper interconnect structures. *Microelectronic Engineering*, 64(1):375–382, 2002. MAM2002.

[54] Z-S. Choi, R. Mönig, and C.V. Thompson. Effects of microstructure on the formation, shape, and motion of voids during electromigration in passivated copper interconnects. *Journal of Materials Research*, 23(2):383–391, 2008.

[55] Baozhen Li, Timothy D Sullivan, Tom C Lee, and Dinesh Badami. Reliability challenges for copper interconnects. *Microelectronics Reliability*, 44(3):365–380, 2004.

[56] Daniele Contestable-Gilkes, Deepak Ramappa, Minseok Oh, and Sailesh M Merchant. Effect of copper seed aging on electroplating-induced defects in copper interconnects. *Journal of electronic materials*, 31(10):1047–1051, 2002.

[57] Young-Joon Park, Jungwoo Joh, Jayhoon Chung, and Srikanth Krishnan. Current crowding impact on electromigration in al interconnects. In *2019 IEEE International Reliability Physics Symposium (IRPS)*, pages 1–6. IEEE, 2019.